Quantitative functionally-defined relationships between structural and functional connectivity within the human brain

by

Kevin Grant Solar

A Thesis submitted to the Faculty of Graduate Studies of

The University of Manitoba

In partial fulfillment of the requirements of the degree of

MASTER OF SCIENCE

Department of Physiology and Pathophysiology

Max Rady College of Medicine

Rady Faculty of Health Sciences

University of Manitoba

Winnipeg, MB

Abstract

Structural connectivity (SC) describes the white matter pathways that provide the electrochemical basis of functional connectivity (FC: temporally-coherent brain activity amongst anatomically-distinct brain regions). Initial human SC-FC relationship studies using magnetic resonance imaging (MRI) were largely exploratory and used only anatomical brain parcellations (failing to account for functional network organization), and revealed that SC reliably predicts FC, but that FC does not appear to predict SC. The purpose of this thesis is to elucidate SC-FC coupling within resting state functional networks. Diffusion tensor and myelin water MRI were applied to measure SC, with resting state functional MRI to measure FC. I tested the strength of SC-FC relationships by linear correlation and regression analyses. This thesis provides novel empirical evidence for divergent and non-overlapping SC-FC coupling within resting state networks, and importantly reveals a few specific brain regions that appear to be disproportionally involved in SC-FC coupling.

Acknowledgements

I want to thank everyone who has been involved up to this point in my graduate career. First and foremost, I would like to thank Dr. Chase Figley and Dr. Jennifer Kornelsen for their willingness to take me on as a Master's student. I feel extremely lucky to have been guided by two such intelligent, passionate and caring people. It has been a great honour to be a part of both the Kornelsen NeuroImaging Lab and the Figley NeuroImaging Lab. I would also like to thank Teresa Figley, Radiology Research Coordinator, for her assistance in the creation of manuscript figures and other general advice. Moreover, I would like to thank the members of my committee, Dr. Katinka Stecina and Dr. Jonathan Marotta, for their valuable time and feedback throughout the past two years.

I would also like to thank the Natural Sciences and Engineering Research Council of Canada for their financial support via the Canada Graduate Scholarship (Masters) for 12 months of my time as a graduate student at the University of Manitoba.

Dedications

There are many people near and dear to me to whom this work is dedicated to. I would like to thank my family, from my grandparents to my parents, for providing their unwavering support and love throughout my academic career. First, I want to dedicate this thesis to my late Baba and Dido who encouraged higher education and greater learning as teachers in Manitoba, and who each completed Master's theses themselves in Education. Next, I want to dedicate this thesis to my Granny and Papa who came from Hungary to Winnipeg in order to establish their family, home and business. Finally, I dedicate this thesis to my Mother and Father who are the best people in my life, and to my little sister, Justine, for putting up with me, and to my sweetest puppy, Leia, for being of great assistance throughout the entire process. I want to thank my Mother and Father for providing me with the life that has allowed me to grow into the proud person that I am today.

Contribution of Authors on Manuscript

Drs. Chase Figley and Susan Courtney acquired this data in Baltimore, Maryland at Johns Hopkins University. Drs. Chase Figley and Jennifer Kornelsen contributed to the revision of the submitted manuscript.

Kevin G. Solar preprocessed and analyzed the data, wrote the manuscript, and created the tables and figures (figures with the assistance of Teresa Figley).

Table of Contents

List of Figures

In Thesis

In Journal Manuscript

List of Abbreviations

3D: Three-dimensional

aSN: Anterior salience network

B_0: External static magnetic field

BOLD: Blood oxygen level dependent

CSF: Cerebrospinal Fluid

Da: Axial diffusivity

dDMN: Dorsal default mode network

DREADD: Designer receptor exclusively activated by designer drug

DREAMM: DREADD-assisted metabolic mapping

Dr: Radial diffusivity

DTI: Diffusion tensor imaging

DV: Dependent variable

EPI: Echo planar imaging

FA: Fractional anisotropy

FC: Functional connectivity

FDG: Fluorodeoxyglucose

fMRI: Functional magnetic resonance imaging

FOV: Field of view

FWHM: Full-width half maximum

GE-EPI: Gradient echo, echo planar imaging

GRASE: Gradient- and spin-echo

ICA: Independent component analysis

IV: Independent variable

JHU: Johns Hopkins University

LDDMM: Large deformation diffeomorphic metric mapping

lECN: Left executive control network

M: Net magnetization vector

MD: Mean diffusivity

MPRAGE: Magnetization prepared rapid acquisition gradient echo

MR: Magnetic resonance

MRI: Magnetic resonance imaging

MWF: Myelin water fraction

MWI: Myelin water imaging

PET: Positron emission tomography

pSN: Posterior salience network

rECN: Right executive control network

RF: Radio frequency

RMP: Resting membrane potential

ROI: Region of interest

rs-fMRI: Resting state functional magnetic resonance imaging

SENSE: Sensitivity encoding

SC: Structural connectivity

SE-EPI: Spin echo, echo-planar imaging

TE: Echo Time

TR: Repetition Time

vDMN: Ventral default mode network

Chapter 1: General Introduction

1.1 Introduction to the Thesis

Understanding the relationships between the wiring of the brain (white matter projections), structural connectivity (SC), and the coordinated firing of the brain (temporally coherent neural activity), functional connectivity (FC), is an essential topic in neuroscience. Prior magnetic resonance imaging (MRI) studies have revealed that strong SC between two brain regions is highly predictive of strong FC between those same regions, but that the reverse is not as reliable, as there are many instances of brain regions with FC but no direct SC between them. These studies are largely exploratory (data-driven) in which SC-FC relationships were examined across the entire brain or sets of select connections using linear regression, correlation, or graph theoretical analyses. They are also limited to the use of anatomically-defined brain regions and strictly diffusion-based MRI methods for the quantification of SC.

The objective of this thesis is to contribute to our understanding of the structural and functional organization of the healthy human brain. SC was quantified using diffusion-based MRI or diffusion tensor imaging (DTI) metrics and myelin water-based MRI or myelin water imaging (MWI) metrics in concert with a functionally-defined human white matter atlas. FC was quantified using blood oxygen level-dependent (BOLD) resting state functional MRI (rs-fMRI) in concert with a complementary fMRI FC atlas. Chapter 1 presents general introduction including various analyses that have been used to measure SC and FC, with a detailed description of MRI techniques, analyses and SC-FC relationship findings. Chapter 2 presents the rationale, objectives and hypotheses for the thesis research project. Chapter 3 presents a manuscript that describes the background, methods, results, and discussion of a series of SC-FC relationship analyses conducted for the completion of this thesis. Chapter 4 presents a brief and

broad discussion of the neuroimaging findings described in the manuscript. Chapter 5 describes important future directions of this research. Chapter 6 presents the concluding remarks of the thesis.

1.2 Structure-Function Relationship Literature

Structure-function relationships are pervasive throughout nature and exist in numerous arrangements. One of the first prominent examples was published by Charles Darwin in the mid-1800s on the finches of the Galapagos Islands whose beak structures determined the types of food that they could forage. In the opposing direction, wherein function seemingly directs structure, Donald Hebb wrote in 1949 how the simultaneous activity or functional connectivity between two neurons increased the strength of the structural connections or synapses between neurons. Since this time, neurophysiological studies have made great strides in understanding structure-function relationships on the microscale: from individual neurons, axons, dendrites and synapses in structural connections to functionally-connected groups of neurons in cortical columns. Microscale studies involve a variety of methods including simple microscopy and staining, as well as more complex approaches such as designer receptor exclusively activated by designer drug (DREADD) technology. However, the macroscale investigation (e.g., at the level of cortical and subcortical regions connected by inter- and intra-hemispheric white matter pathways) of structure-function coupling has just recently gained traction throughout the last decade by the application of advanced MRI techniques. SC, or the long distance white matter projections and bundles that connect anatomically distinct regions of the brain, can be quantified using a number of MRI methods including DTI and MWI. FC, or temporally-coherent brain activity amongst anatomically-distinct regions, can be quantified using rs-fMRI that measures

spontaneous fluctuations in the BOLD signal (an indirect measure of brain activity). In order to understand how neural communication and integration of information works across different parts of the brain, it is important to understand how SC couples with FC at the macroscale as well as the microscale.

1.2.1 Microscale Structure-Function Relationships

Although this thesis focuses on macroscale structure-function relationships, I will provide a brief review in this subsection regarding microscale investigations. The earliest examinations of structural and functional relationships on the microscale involved microscopy to examine structure and electrophysiology to study function. Cytoarchitecture involves the classification of brain anatomy or structure via *in vitro* microscopic examination; and it has been a topic of interest for more than a century (Barbas, 2015; Broadmann, 1909; Campbell, 1903; Roland et al., 1997; Von Economo & Koskinas, 1925; Zilles et al., 2015). Cytoarchitecture studies suggest that variation in structure at the microscale level coincides with functional roles through structural-functional coupling within the human cortex (Amunts & Zilles, 2012; Barbas, 2015; Zilles et al., 2015). For instance, the human cortex is organized in a series of six distinct layers, each with their own characteristic neuronal cell types and connections (Broadmann, 1909; Von Economo & Koskinas, 1925). Histological staining of neural tissue is also popular for distinguishing structural and functional areas. Staining techniques work by using a chemical or antibody that binds to specific structures within the brain. For example, Golgi staining allows investigators to highlight the dendrites of neurons and trace their connections. In terms of structure-function relationships, cytoarchitecture and staining studies have revealed, for example, that the functional diversity of associative brain regions is reflected in its neuronal organization wherein

pyramidal neurons are larger in size and have more branching and spikes relative to other neurons of the sensory or motor cortices (Elston, 2003; van den Heuvel et al., 2015; Yuste, 2011).

Electrophysiological approaches have also been integral to understanding brain structure in relation to function on the microscale. By manipulating internal membrane factors and external inputs from neurotransmitters and modulators *in vitro*, electrophysiological recordings from brain slices reveal the function of different structures in healthy and in disease states. In such studies, brain slices are stimulated electrically or chemically. For example, functional subfields of the hippocampus were characterized using glutamate stimulation in a seminal study (Christian et al., 1988). These researchers found that one particular subfield, CA1, had longer excitatory connections in the transverse than in the longitudinal plane. Moreover, these excitatory connections were denser than those found in another subfield, CA3. This finding aligns with behavioural studies that demonstrate, amongst many similar functions, that CA1 is involved in contextual memory retrieval, while CA3 is not (Knierim, 2015). Overall, on the microscale, there seems to be a structure-function relationship in which the more complex the structure is in terms of cell types and cellular arrangements, the more diverse functionalities it can serve.

Genetics-based approaches have recently gained popularity in extending our knowledge of the diverse functions of the human brain on the microscale. For instance, we can use DREADD technology combined with μ-positron emission tomography (μPET) and [18F] fluorodeoxyglucose (FDG) to generate whole-brain metabolic maps of cell-specific functions, which is referred to as DREADD-assisted metabolic mapping (DREAMM) (Ferguson & Neumaier, 2015; Michaelides et al., 2013). DREAMM is a high-resolution, molecular imaging method that allows for *in vivo* control of cell-specific firing through the DREADDs technique,

and utilizes functional brain imaging using μPET with FDG as an indirect marker of corresponding neuronal activity (Michaelides et al., 2013). In a seminal DREAMM study, investigators identified distinct microscale functional networks associated with normal and pathologic behaviour (Michaelides et al., 2013). DREAMM is an extremely promising technique in the field of neuroscience, specifically in understanding structure-function relationships, as it allows for *in vivo,* temporal, microscale, whole-brain activity mapping in response to specific neuronal manipulations (Michaelides et al., 2013). It is important to continue exploring the utility of DREAMM as it should allow researchers to make more causality-based links between microscale structure and function in the brain.

1.2.2 Macroscale Structure-Function Relationships

1.2.2.1 Structural Connectivity

SC can be quantified using a number of MRI methods, but for the purpose of this thesis, I will focus on DTI and MWI; and I will provide a qualitative description of these techniques in the current section, followed by a more technical discussion in section *1.3 General Principles and Underlying Physiology of Magnetic Resonance Imaging* of this thesis. Diffusion-weighted imaging is a non-invasive MRI technique that is sensitive to the 3D movement and diffusion rate of water in brain tissue and can be used to quantify SC. One of the earliest studies to examine water diffusion in the healthy human brain was by Thomsen et al. (1987), which revealed clear differences in diffusion between grey and white matter regions. The researchers proposed that the manner of diffusion depends on the microstructure of the brain: wherein water diffuses easily along the path parallel to the white matter tract direction but is highly impeded along paths that are perpendicular to the tract. This situation occurs due to the inability of water to diffuse

through the hydrophobic fatty cells that make up the myelin sheaths of white matter tracts. DTI is an MRI technique that models this water-diffusion information as a 3D brain image. DTI, first described by Basser et al. (1994), allows us to image the white matter tracts of the human brain by taking advantage of the fact that the water within our bodies is constantly moving due to Brownian motion, and in turn is always diffusing internally, externally, and through the cellular structures of various tissues. Within white matter pathways or neural fibres, largely anisotropic water diffusion is found due to dense populations of axons covered with their myelin sheaths. Myelin allows for fast, saltatory conduction, but also provides a strong barrier to diffusion due to the limited water permeability of the hydrophobic lipid bilayers that make up myelin membranes (Beaulieu, 2002). Within gray matter however, the dense microstructure is not as orderly as in white matter, so water molecules diffuse in many directions, thus diffusion in gray matter is isotropic. DTI can produce a number of different metrics of SC and some of the most commonly used include fractional anisotropy (FA), mean diffusivity (MD), radial diffusivity (Dr) and axial diffusivity (Da) (Alexander et al., 2007). For the purposes of this thesis, I will focus on FA which measures the microstructural integrity of white matter tracts and MD, which measures the membrane density of white matter tracts.

Moreover, histopathological validity has been confirmed in DTI: a study used DTI to predict the quantitative analysis of microphotographs produced from temporal lobe epilepsy patients who underwent temporal lobe resections (Concha et al., 2010). Prior to surgery, patients underwent a DTI scan; and the researchers found that the morphological results of the electron microscopy analysis of the excised tissue correlated strongly with the DTI-based metrics (FA and MD) extracted non-invasively from the same tissue prior to excision. This study (Concha et al., 2010) provides important validity to DTI as a means of quantifying SC.

SC can also be quantified using MWI, which is a non-invasive MRI technique that is sensitive to the fraction of water molecules trapped within the myelin layers that make up white matter tracts of the human brain. MWI takes advantage of the fact that the magnetic resonance (MR) signal varies between water trapped within the layers of myelin sheaths, water trapped in intra- and extra- cellular compartments throughout the brain, and water within the cerebrospinal fluid (CSF). In a seminal MWI study by Whittall et al. (1997), the investigators calculated the myelin water fraction (MWF) as a metric of SC, which measures how much myelin is present in a particular white matter tract by dividing the MR signal from the myelin water of the brain to that of the total water in the brain tissue (intra- and extra- cellular compartments, but not CSF). In Whittall et al. (1997), the average MWF was extracted from 12 white and gray matter regions using a region of interest (ROI) analysis (which is detailed in section *1.5.1 Structural Connectivity Data Analysis*). Importantly, the results of this study revealed that the MWF was significantly higher for all white-matter structures relative to all grey-matter structures (Whittall et al., 1997).

Overall, there are some general differences between SC imaging modalities. In DTI, FA and MD are more-general measures of SC strength that are only partly determined by the presence of myelin as an indicator of SC: they measure water diffusion properties and water diffusion is restricted in varying degrees by not only myelin and membrane density. For instance, a seminal study found that a non-myelinated nerve can also be traced using DTI (Beaulieu & Allen, 1994), indicating that some structural aspects of the axons, other than myelination, influence anisotropy. However, myelin does indeed contribute to DTI measures as SC would be quantified as stronger in a myelinated axon relative to an otherwise similar axon without myelin (Beaulieu, 2002). In

MWI, the MWF specifically measures the myelin content of white matter tracts in order to quantify SC.

Studies that have examined the SC and SC-FC relationships of the human brain have mainly focused on DTI measurements (Harriger et al., 2012; Senden et al., 2014; Stam & van Straaten, 2012; van den Heuvel & Sporns, 2011). Early studies found that SC is organized into a whole-brain network topology, rather than being a simple summation of the individual regions and connections, and that it is this whole-brain SC network which makes global brain communication and FC possible (Bullmore & Sporns, 2009; Sporns et al., 2005). The notion of small-world network organization was put forth by Bassett & Bullmore (2006) who suggested that there are multiple SC networks organized into few distributed, locally clustered groups of regions and connections. Amongst these SC networks are a number of regions, including the precuneus and superior frontal regions, which have been identified as brain hubs due to their participation in a disproportionately high number of structural connections (Sporns et al., 2007; van den Heuvel et al., 2010).

The idea of brain hubs has now been extended to include a group of brain regions and connections that are not only rich in connections to other regions like the brain hubs described above but are also highly connected to one another, forming a club – these are referred to as the 'rich club' (van den Heuvel et al., 2012; van den Heuvel & Sporns, 2011). The rich club has been replicated in multiple studies that show it includes bilateral precuneus, superior frontal and temporal cortex, hippocampus, thalamus and putamen (Collin et al., 2014; Senden et al., 2014; van den Heuvel et al., 2012; van den Heuvel & Sporns, 2011). These rich club regions and the connections amongst them, called the rich club network, are thought to provide the structural or anatomical substrate that facilitates global brain functional connectivity (Collin et al., 2014;

Senden et al., 2014; van den Heuvel & Sporns, 2013) – a notion that is supported by the fact that well-established resting state FC networks, including the default mode network (DMN), executive control network (ECN) and salience network (SN; which are described in the next section), have multiple nodes that are located within rich club regions (Figley et al., 2015; Senden et al., 2014; van den Heuvel & Sporns, 2011).

1.2.2.2 Functional Connectivity

In terms of macroscale function, I will focus on BOLD-based fMRI (Ogawa et al., 1990). Unlike structural imaging techniques such as DTI and MWI that simply provide spatial information about brain structure, fMRI provides both spatial and temporal information about neural activity, allowing researchers to track neural activity throughout the brain over the scan duration. There are multiple fMRI techniques that are sensitive to different aspects of neural activity, such as blood flow and volume as well as the metabolic rate of oxygen consumption, however BOLD-based fMRI depends on differences in the magnetic susceptibility of oxygenated versus deoxygenated hemoglobin (Huettel, 2004; Ogawa et al., 1990). I focused on Huettel (2004) to build an understanding of fMRI.

The theory behind the BOLD signal begins with the fact that when neurons are activated, ions move across their membranes in order to send/receive electrochemical signals in a process that disrupts the resting membrane potential (RMP) of the active neurons (Huettel, 2004). Once the membrane potential is no longer at the RMP, the neuron must return to the RMP in order to be ready for further activity that is accomplished by an active pump that requires energy in the form of adenosine triphosphate (ATP), which pumps potassium ions into the neuron while sodium ions are pumped out (Huettel, 2004). The greatest source of ATP in the brain is through

aerobic respiration that requires oxygen (Caballero, 2013). According to Huettel (2004), due to neurovascular coupling, an increase in neural activity in a population of neurons is followed by a hemodynamic response that involves vasodilation, an increase in blood flow, and a decrease in the ratio of deoxygenated hemoglobin to oxygenated hemoglobin after the capillary bed associated with the neuronal population that was just active. This hemodynamic response involves a surge of oxygen, more than is needed by the active neuronal population to restore RMP, which leaves some 'left-over' oxygenated hemoglobin in the blood vessels following the capillary bed of the active neuronal population. The essential feature of the BOLD signal, which leads to image contrast that corresponds to neural activity, is the difference in magnetic susceptibility between deoxyhemoglobin and oxyhemoglobin: 1) deoxyhemoglobin is paramagnetic (larger, positive susceptibility to magnetic fields: distorts MR images), and 2) oxyhemoglobin is diamagnetic (weak, negative susceptibility to magnetic fields: does not distort MR images; Huettel, 2004). Therefore, a decrease in the ratio of deoxyhemoglobin to oxyhemoglobin following neural activity will result in a decrease in the presence of distortion-causing molecules, therefore increasing the MR signal at the area of neuronal activity. FC is defined by anatomically-distinct regions of the brain whose BOLD MR signal is temporally correlated (i.e., brain regions with neural activity that fluctuated up and down together throughout the scan; Honey et al., 2010). In turn, a large-scale functional or FC network is defined as a group of spatially- or anatomically-distinct regions, or network nodes, in the brain whose BOLD MR signal is temporally correlated (Bressler & Menon, 2010).

Resting State Functional Magnetic Resonance Imaging: Functional MRI can be used to characterize neural activity through two basic approaches: 1) in response to a task or stimulus, in what is referred to as task-based fMRI, and 2) during rest in the absence of explicit input or

output (subject's eyes are closed, open, or open and fixated on a cross), in what is referred to as rs-fMRI. In a seminal study regarding the resting state of the human brain by Fox & Raichle (1986), researchers using positron emission tomography found that despite an increase in cerebral blood flow during a somatosensory-stimulation task relative to a resting state condition (in which subjects had their eyes closed), there was no significant difference between metabolic oxygen consumption. This finding suggests that the brain consumes similar amounts of energy and therefore experiences similar levels of neural activity during both an explicit task and while at rest. This study notably demonstrates that although a person is at rest (not engaged in any cognitive, language, or motor activities), the brain is still active to a degree that is not unlike the activity observed during an explicit task and is not due to simple autonomic functions like heartbeat or respiration (Fox & Raichle, 1986). The earliest report of rs-fMRI by Biswal et al. (1995), however did not appear for about another decade. In the Biswal et al. (1995) study, subjects were imaged at rest and during task-engagement. While the subjects were at rest, the researchers identified several spatially-distinct brain regions with temporally-correlated BOLD signals, which together composed a resting state functional network. This network consisted of several nodes located in regions such as the left sensorimotor cortex and the premotor area, in what is now referred to as the sensorimotor resting state functional network.

A number of different resting state networks have been identified in relation to different sensory, cognitive and behavioural functions (Shirer et al., 2012). Three of the most common and well-established resting state networks include the DMN, ECN and SN. They are often studied in halves because; 1) that is how they are identified in fMRI experiments (Shirer et al., 2012), and 2) to reduce computational time: dorsal and ventral DMN (dDMN, vDMN), left and right ECN (lECN, rECN), and anterior and posterior SN (aSN, pSN). The DMN is involved in self-

referential thinking, emotional processing, and memory recall (Buckner et al., 2008). The DMN includes network nodes located in the posterior cingulate cortex, precuneus, angular gyrus, and the lateral parietal lobe. Also, it is referred to as a 'task-negative' network due to the suppression of activity in associated brain regions during engagement in cognitive, perceptual or behavioural tasks (Buckner et al., 2008).

The other two networks, ECN and SN are referred to as 'task-positive' networks because the activity increases in these networks during engagement in relevant tasks. The ECN becomes active during executive functioning tasks such as planning for the future and problem solving, and it includes nodes in the middle and superior frontal gyri (Seeley et al., 2007). The SN is responsible for distinguishing and shifting attention to pertinent environmental stimuli, and it utilizes nodes located in the insula, anterior cingulate cortex, precuneus and thalamus (Seeley et al., 2007). Changes in the connectivity of these networks have been associated with human diseases such as in people with autism who demonstrate 'overconnectivity' (higher than normal FC) in the DMN and rECN and 'underconnectivity' (lower than normal FC) in the SN and lECN (Abbott et al., 2016). It is therefore important to delineate the SC-FC relationships that sustain these networks in the healthy human brain so that we may begin to understand such diseases.

1.2.2.3 Structural-Functional Connectivity Relationships

Initial investigations of structural-functional connectivity relationships using MRI techniques were relatively basic and largely qualitative in that their goal was to simply establish the presence/absence of structural connections between functionally-connected brain regions in resting state networks (Damoiseaux & Greicius, 2009; De Luca et al., 2006; Toosy et al., 2004; van den Heuvel et al., 2009), rather than looking at correlations between strength of SC and FC.

This was commonly accomplished by running DTI tractography between target brain regions to establish whether or not there was robust SC in concordance with the presence or absence of FC as measured using rs-fMRI. These early studies converged on the notion that brain regions with SC should show FC, but that the reverse does not hold as strong since there are often regions identified with FC but no direct SC, suggesting: 1) current techniques cannot resolve all structural connections, and 2) some functional connections may be indirectly supported by some third party. Quantitative assessments of SC have gained more traction recently in SC-FC coupling investigations; and these involve simple measurements such as the number of white matter streams and the length of those streams (Hagmann et al., 2008; Hermundstad et al., 2013, 2014; Honey et al., 2009; Huang & Ding, 2016) to more complex diffusion-based metrics such as FA (Huang & Ding, 2016; Khalsa et al., 2014; Toosy et al., 2004; van den Heuvel et al., 2008). There are some slight inconsistencies amongst the quantitative findings. For example, an early study by van den Heuvel et al. found that mean FA as a measure of SC strength for the white matter pathway from the posterior cingulate cortex to medial frontal cortex was highly associated with FC strength for the same pair of regions (van den Heuvel et al., 2008). However, a more recent investigation of the same brain regions revealed that the number of streamlines as a measure of SC strength, but not FA, was directly correlated with FC (Huang & Ding, 2016). In whole brain studies, there is strong direct coherence between SC and FC, and despite some inconsistencies within specific connections, these studies converge on the extended notion that the strength of SC is directly associated with that of FC for a given pair of brain regions.

All of these previous MRI-based investigations of SC-FC relationships in the human brain have largely focused either on the whole-brain (Hagmann et al., 2008; Honey et al., 2009; Meier et al., 2016; Mišić et al., 2016; Skudlarski et al., 2008; Stam et al., 2016; Tewarie et al., 2014) or

on a few specific brain regions (Greicius et al., 2009; Huang & Ding, 2016; Khalsa et al., 2014; van den Heuvel et al., 2009, 2008). The whole-brain approach is data-driven in that it involves compiling SC and FC data (using whole-brain DTI and rs-fMRI scans), running relationship analyses (e.g., linear correlational analyses, graph theory analyses) and examining the trends throughout the entire data set. These prior studies also commonly used an anatomical-parcellations in which the brain was divided using anatomical or structurally-defined coordinates. Different studies have used varying degrees of resolution and different analyses in their anatomical-parcellations. For instance Skudlarski et al. (2008) applied 6,000 voxels in a voxel-wise approach, whereas Honey et al. (2009) used 66 cortical regions-of-interest (ROIs) as well as a finer 998 cortical ROI parcellation, the same as used in Hagmann et al. (2008). These investigations only speak to SC-FC relationships within anatomically-defined brain regions; and although these approaches are fruitful, they fail to consider a fundamental aspect of human brain organization: the division into functionally-distinct networks in which the component regions (nodes) are not necessarily defined by anatomical boundaries but rather by their spread of activation, which may cross multiple anatomical regions or only involve a portion of a total region. Therefore, it is important for studies to examine SC-FC coupling between functionally-defined network nodes.

It is important to mention that some studies have investigated SC-FC relationships within resting state FC networks by extracting functional network patterns from their rs-fMRI data (Hagmann et al., 2008; Mišić et al., 2016; Skudlarski et al., 2008; Stam et al., 2016) and looked at how SC relates to these patterns. While these studies provide some insight regarding SC-FC coupling within resting state networks, they still base those networks upon anatomical coordinates, rather than purely functionally-defined nodes. In order to understand how SC in the

human brain supports FC within resting state networks, it is important to investigate the SC-FC relationships amongst the functionally-defined nodes that comprise these networks. Through the application of corresponding functionally-defined structural (UManitoba-JHU Functionally-Defined Human White Matter Atlases; Figley et al., 2015) and functional (Stanford fMRI Atlases; Shirer et al., 2012) MRI atlases of six well-established resting state networks, I was able to conduct a novel systematic analysis of SC-FC coupling within strictly functionally-defined brain regions.

It should also be mentioned that the majority of these previous SC-FC studies have also been limited to a single SC imaging modality: DTI. Moreover, most studies only utilize the number of fibres or FA as DTI-based measures of SC (Honey et al., 2009; Huang & Ding, 2016; van den Heuvel et al., 2008). Few, if any studies, have utilized a multimodal approach that incorporate multiple SC imaging methods such as MWI in addition to DTI. Such an approach should provide greater validity to the SC-FC relationships identified, as well as to the multimodal methods used. In the current thesis, I quantify SC using DTI-based FA and MD as well as MWI-based MWF.

The importance of understanding SC-FC coupling at the macroscale is magnified by studies that have found that many human illnesses are associated with changes in SC-FC coupling, including various types of multiple sclerosis (Akbar et al., 2016; Zhou et al., 2014), Alzheimer's disease (Sun et al., 2014), temporal lobe epilepsy (Chiang et al., 2015), and major depressive disorder (Kwaasteniet et al., 2012). The multiple sclerosis studies compared patients with pediatric onset multiple sclerosis (Akbar et al., 2016) and relapsing remitting multiple sclerosis (Zhou et al., 2014) types to neurologically-healthy controls, and examined brain regions associated with the DMN (e.g., posterior cingulate cortex/precuneus, medial prefrontal cortex), the increased FC of which is positively associated with the severity of multiple sclerosis

symptoms (Hawellek et al., 2011; Rocca et al., 2010). These studies revealed that both pediatric onset and relapsing remitting multiple sclerosis patients show significant SC-FC decoupling in which FC is increased in the DMN where SC has deteriorated (Akbar et al., 2016; Zhou et al., 2014). SC-FC decoupling was also found in patients with Alzheimer's disease (Sun et al., 2014), major depressive disorder (Kwaasteniet et al., 2012), and temporal lobe epilepsy (Chiang et al., 2015); and in each of these illnesses, SC was found to decrease as FC increased. The investigators propose that there may be a compensatory neural activation mechanism in which loss of white matter microstructural integrity is compensated by stronger FC. In order to understand such a mechanism, it is imperative that we elucidate normal SC-FC coupling in neurologically-healthy individuals.

1.3 General Principles and Underlying Physiology of Magnetic Resonance Imaging

MRI is a non-invasive imaging modality that is sensitive to a wide-range of tissue properties by disturbing various atomic nuclei within the body. The common nucleus of choice in MRI is that of hydrogen because it is the most plentiful atom in the body due to the abundance of water (made up of two hydrogens and one oxygen) found in human tissues. Each hydrogen nucleus is made up of a single (positively-charged) proton, the spinning of which creates a small current on its surface that in turn produces a small magnetic field and torque when placed inside a large magnetic field; this effect is called the magnetic moment (Huettel, 2004). The single proton of hydrogen also has an atomic mass so that the spinning creates angular momentum (Huettel, 2004). Under normal conditions (not inside a strong magnetic field), the hydrogen spins (protons) are randomly oriented throughout the body, causing the individual magnetic moments to cancel out, resulting in a net magnetization that is nearly zero (Huettel, 2004).

The net magnetization of hydrogen protons in the target brain volume needs to be increased for an MRI scan (Huettel, 2004). This requirement is accomplished in the first major step of MRI often referred to as 'preparation' in which a strong external static magnetic field (B_0) is applied to the body; and it is this main magnetic field that constitutes the "M" in MRI. When hydrogen protons are placed into this external magnetic field, they begin to move in a gyroscopic manner known as 'precession' (imagine a spinning top which spins around its vertical axis and wobbles out of line with this axis so that the top-end traces a circle around the axis; this wobble is like precession; Huettel, 2004). The application of a constant external magnetic field will cause protons to precess at the same frequency, referred to as the Larmor frequency, which is proportional to the magnetic field strength. Of these, there are slightly more protons that precess parallel to the direction of B_0 (along what is often referenced as the z-axis, running parallel to the bore of the MRI scanner) in the lowest-energy state than those that precess anti-parallel to the direction of B_0 in the second lowest-energy state (Huettel, 2004). As a result, the sum of the magnetic moments of every proton in B_0, referred to as the net magnetization vector (M) is comprised of a longitudinal component that runs parallel to B_0 (in the z-axis). The transverse component of M is effectively zero because the transverse components (in the x- and y- axes, perpendicular to B_0 in the z-axis) of each proton's individual magnetic moment cancel out due to the fact that they precess out-of-phase in great numbers (Huettel, 2004). Establishing an equilibrium state with net magnetization under B_0 marks the end of the first step, 'preparation'.

Now that the net magnetization of the hydrogen protons has been increased, its equilibrium state must be disturbed in order for the protons to become visible to the MRI scanner: the net magnetization must be tipped from the longitudinal plane (where precession cannot be measured) and into the transverse plane (where precession can be measured). This second step is referred to

as ‘excitation’ due to the fact that it involves transferring energy to the protons’ atomic nucleus at their resonance frequency so that some flip from lower- to higher-energy states; and it is this step that defines the “R” in MRI. When oscillating magnetic fields at the Lamour frequency – corresponding to the radio frequency (RF) – are applied, some protons will flip from the lower- to the higher-energy state and begin precessing in-phase in the transverse plane. Once there are equal amounts of protons in the low- and high-energy states, the longitudinal net magnetization vector sums to zero because it has been transferred to the transverse vector that is now greater than zero and is detectable as an MR signal. This energy transference is made possible by using resonance RF waves tuned to oscillate at the same frequency at which the protons precess in a relationship defined by the Larmor Equation:

$$\omega_0 = \gamma B_0$$

in which ω_0 defines the resonant frequency, γ defines the gyromagnetic constant, and B_0 defines the strength of the static magnetic field. According to this equation, the resonant frequency at which the protons precess is directly proportional to the strength of the static magnetic field. The application of an excitatory RF pulse (from RF coils in the MRI scanner that are tuned to the resonant frequency) effectively forces proton spins into phase so that they precess together (same phase and frequency) in the transverse plane. The termination of the RF pulse signifies the end of the ‘excitation’ stage.

Although the equilibrium state of the protons has been disrupted, it will begin to restore itself once the RF pulse is removed as the excess high-energy spins return to low-energy states and as individual spins de-phase. However, while these ‘excited’ or ‘disrupted’ protons are precessing with the same frequency and phase, the transverse vector of the net magnetization creates electromagnetic oscillations at the Larmor frequency that induce changing current in RF

receiver coils; and it is this changing current that comprises the MR signal that is acquired and ultimately transformed into brain images, hence the "I" in MRI.

During this final stage, the protons that were excited will relax by returning from a high- (anti-parallel to B_0) to a low-energy state (parallel to B_0) and losing their in-phase character by beginning to precess out-of-phase again. There are two main types of relaxation or important changes in magnetization that occur after the RF excitation pulse is turned off and can be used as weighting in the image contrast: 1) T_1-relaxation that involves an increase in the longitudinal net magnetization vector as the protons realign with B_0, and 2) T_2-relaxation that involves a decrease in the transverse net magnetization vector as the protons de-phase and cancel each other out. T_1- and T_2- relaxation both begin as soon as excitation ceases, function with different time constants, and are dependent on varying characteristics of the tissue being imaged – therefore making it possible to generate many different types of images using an MRI scanner by varying the amounts of T_1 and T_2 image contrast.

There are two key scanning parameters that are involved in determining the type of image that is produced in an MRI scan: 1) repetition time (TR), which is the time between RF pulses, and 2) echo time (TE), which is the time between the end of the RF pulse and MR signal acquisition; and they are both defined on the order of milliseconds. Shorter TRs impart more T_1 image contrast, whereas longer TEs impart more T_2-weighted image contrast. Due to the fact that diverse tissues have different characteristics that effect relaxation times, (e.g., varying levels of water, fat and magnetic susceptibility), coupled with the capability to manipulate the way in which we apply excitation and image acquisition through varying MR pulse sequences, there are many different MRI techniques that have emerged.

In order to generate a coherent image in 3D space, a crucial part of the excitation and acquisition steps is the localization of the MR signal in 3D space through 'spatial encoding' procedures that are accomplished by applying additional magnetic field gradients in the x, y, and z directions. For example, within an MRI scanner the brain can first be divided into axial slices along the z-axis of the scanner (in the horizontal anatomical plane, from the top/bottom of the head to the bottom/top) using a 'slice selection gradient' and then spatial information is encoded orthogonally to the slice selection gradient along rows and columns within each slice using 'phase encoding' and 'frequency encoding' gradients along the x and y axes. The application of a magnetic gradient will change the Larmor frequency of the protons within the targeted volume. It is then followed by an RF pulse tuned to the new Larmor frequency in order to excite only the protons within the volume defined by the gradients. The slice selection gradient is used during the excitation step in order to excite pre-defined axial slabs of the head along the z-axis. Then, in the first orthogonal direction, frequency encoding is applied so that proton spins in different locations down the x-axis within each slice precessing at different frequencies. Next, in the second orthogonal direction, phase encoding is applied so that proton spins in different locations down the y-axis within each slice precessing in different phases. At this point, proton spins within the 3D brain volume have been spatially differentiated in all three dimensions, thus allowing MRI researchers to localize the MR signal in 3D space.

The ability to image hydrogen within the brain can be exploited in many ways by using different scan or pulse sequences; and for the purpose of this thesis, three different MRI techniques (which were used in the current study) are detailed below. The first two, DTI and MWI are used to measure the SC of the brain, and the third – rs-fMRI – is used to measure FC.

1.3.1 Diffusion Tensor Imaging

In a common diffusion tensor imaging (DTI) scan (as was used in the current thesis), a single-shot spin echo, echo-planar imaging (SE-EPI) pulse sequence is often used with an additional set of diffusion-encoding magnetic field gradients that are applied in many different directions (needs to be at least 6 directions, but 30 or more directions is now standard) in order to sensitize the signal to the water diffusion with respect to each diffusion-encoding gradient (Alexander et al., 2007). Overall, a number (6+) of diffusion-weighted images are produced alongside a smaller number of anatomical T_2-weighted non-diffusion images. The water molecules that were moving through each magnetic gradient will have different magnetization in comparison to other nearby water molecules and will produce a corresponding change in image contrast. The combination of the direction with the amount of water diffusion allow for the calculation of a tensor, which is an ellipsoid based on the amount and direction of diffusion (Basser et al., 1994). The tensors that are calculated throughout the entire brain during a DTI scan can be quantified using different metrics, such as FA subject maps that quantify how isotropic the tensors are throughout the brain, and MD subject maps that quantify the average magnitude of water diffusion within the tensors throughout the brain. In order to quantify SC, FA serves as a measure of the microstructural integrity of white matter tracts, whereas MD serves as an inverse measure of membrane density (Alexander et al., 2007; Feldman et al., 2014). High FA is indicative of strong SC because it implies that water diffusion was highly anisotropic (in one direction) that indicates its movement along a well-defined structural pathway or white matter tract with high microstructural integrity. Whereas a low FA results from highly isotropic water movement, which is indicative of no single definite direction for water diffusion due to low microstructural integrity and/or low directional consistency of the fibers in the white matter

tract (weak SC). On the other hand, low MD values result from highly-restricted water diffusion due to high membrane density, which is indicative of diffusion within a well-defined white matter tract, and thus lower MD corresponds to stronger SC. High MD results from lower average (across directions) membrane density, which is indicative reduced microstructural integrity. FA and MD values can be extracted from the brain using two basic analysis methods: voxel-wise analysis and region-of-interest (ROI) -based analysis, which are detailed below in section *1.5 Magnetic Resonance Imaging Data Analysis*. ROI analyses were applied in the current project.

A unique and essential feature of DTI is that by providing water diffusion information regarding the extent of diffusion anisotropy as well as its orientation, the individual tensors collected throughout the brain can be constructed into coherent 3D objects that represent white matter fibre pathways (Mori & Van Zijl, 2002). A researcher can choose either structurally- or functionally-defined ROIs within the brain from which to manually or automatically (using a variety of computer algorithms) trace fibres using a process called 'fibre tracking' or 'tractography'. Once a tract is defined either in a single subject or in a group of subjects, it can be saved as a new ROI. A researcher can then apply the resulting ROI to any structural MRI data in order to quantify the SC strength of that tract by extracting, for example, the average FA or MD values.

1.3.2 Myelin Water Imaging

MWI utilizes a scanning sequence, commonly a gradient and spin-echo (GRASE) sequence as used in this thesis, which is sensitive to the amount of water that is trapped between the lipid bilayers that make up the myelin sheaths of white matter tracts (Alonso-Ortiz et al., 2015). From

MWI data, a MWF map can be calculated (described above in full in section *1.2.2.1 Structural Connectivity*) from which one can derive SC strength in a particular voxel or white matter tract (collection of voxels in an ROI), wherein a higher MWF indicates stronger SC because more myelinated white matter pathways will trap more water relative to less myelinated pathways (Alonso-Ortiz et al., 2015). Like with DTI data, MWF values can be extracted from the brain using two basic analysis methods: voxel-wise and ROI-based analysis, which are detailed below in section *1.5 Magnetic Resonance Imaging Data Analysis*. ROI analyses were applied in the current project.

1.3.3 Functional Magnetic Resonance Imaging

The scan sequence that is most commonly used for functional-MRI (fMRI) is referred to as gradient echo, echo planar imaging (GE-EPI), which is sensitive BOLD signal. The GE-EPI scan is used to create a timeseries of images over the scan interval and reveals regions of the brain that are functionally connected. FC values can be extracted from rs-fMRI data using three different basic analysis methods: voxel-wise, seed-based, and independent components analysis (ICA), which are detailed below in section *1.5.2 Functional Connectivity Data Analysis*. Seed-based FC analyses were applied in the current project. Within seed-based analyses, a number of different metrics can be calculated as a measure of FC strength between a pair of brain regions, but I will focus on one of the most common, the 'bivariate correlation', which is what I used in this thesis and is described below in full within section *1.5.2 Functional Connectivity Data Analysis.*

A notable limitation of BOLD rs-fMRI FC data is ambiguity, which is rooted in the fact that the BOLD signal provides an *indirect* measure of neural activity (Buckner et al., 2013). For instance, there is uncertainty regarding how FC results that include networks within networks

and anti-correlations should be interpreted in relation to the underlying physiology and anatomy (Buckner et al., 2013; Cole et al., 2010). It is also worth mentioning that fMRI-based FC analyses have low spatial resolution and are only capable of revealing macroscale neural activity (Craddock et al., 2014).

1.4 Magnetic Resonance Imaging Data Preprocessing

The raw brain imaging data, both structural and functional, that are produced by an MRI scanner must be preprocessed prior to any statistical analyses. Preprocessing involves various computational measures to increase the quality, validity and reliability of the acquired data. Preprocessing procedures for MRI data vary within and between different imaging modalities. With an abundance of preprocessing techniques and available software packages to perform them on, an important practice is to use the same structural or functional 'preprocessing pipeline' (software included) for all data of each type within a single MRI study so that results are consistent. In the following three subsections, common preprocessing steps for DTI, MWI and rs-fMRI are described. A step common to each is referred to as 'normalization' in which subject images are warped into a standard space (since everyone's brain is shaped and sized slightly differently), ensuring all data are in the same stereotactic space so that valid and reliable between-subject and group analyses can be conducted.

1.4.1 Diffusion Tensor Imaging Data Preprocessing

The first common step in preprocessing DTI data is to correct for distortions caused by 'eddy currents', circular electrical currents induced by the changing magnetic fields, which are common during diffusion MRI pulse sequences. Within a single subject, eddy current correction

proceeds with affine registration of the diffusion-weighted images (6+) to one of the anatomical T_2-weighted images acquired during the non-diffusion-weighted part of the pulse sequence that will not be subjected to the same distortions caused by the diffusion gradients. Affine registration will correct for geometric distortions in the diffusion-weighted images using the anatomical T_2-wieghted image. Since the DTI scan takes several minutes, the subject is bound to not stay completely still in the scanner and movement creates distortions or artifacts, so the next step in the DTI preprocessing pipeline is 'motion correction'. This step is completed through rigid body registration of all the diffusion-weighted images to an anatomical T_2-weighted image. Next, the non-brain areas of the head that were captured in the scan are removed using an automated procedure (sometimes followed by a manual refinement procedure) wherein the anatomical T_2-weighted and diffusion-weighted images are stripped of non-brain areas. Finally, a normalization procedure (or a series of procedures) is used in which all images are warped to a standard space/template in order to overcome individual variability in brain structure, which is extremely important when conducting between-subject and group analyses.

1.4.2 Myelin Water Imaging Data Preprocessing

The first common step in preprocessing MWI data is the co-registration of a subject's T_2-weighted myelin water images to the same subject's T_1-weighted high-resolution anatomical image. This step corrects for motion and is necessary to ensure that each myelin water image is in the same space/orientation (minimizing the variability between images). Next, the T_1-weighted anatomical image and the T_2-weighed myelin water images are resliced so that they are all the same size and resolution. To proceed, the non-brain areas of the head that were captured in the scan must be removed using an automated procedure (sometimes followed by a manual

refinement procedure) wherein the anatomical T_1-weighted image is stripped of non-brain areas, a corresponding mask is created, and that mask is then applied to strip the same sections from all of the myelin water images. Finally, a spatial normalization procedure (or a series of procedures) is used in which all images are warped to a standard space/template in order to overcome individual variability in individual brain structure, which is extremely important when conducting between-subject and group analyses.

1.4.3 Resting State Functional Magnetic Resonance Imaging Data Preprocessing

The first common step in preprocessing rs-fMRI data is referred to as 'slice time correction' that corrects for the fact that each slice of the 3D brain volume was obtained at a slightly different time (one after another) by using temporal interpolation to adjust the series of images so that all slices appear as if captured at the same time. The next step is to correct for subject movement during the scan. This requirement is accomplished by realigning all of the functional images (also referred to as the fMRI time series) to the mean T_{2*}-weighted image, thus adjusting the fMRI time series so the head is always in the same position and orientation in each image. Following realignment is co-registration of the fMRI time series to the high-resolution anatomical T_1-weighted image from the same subject in order to map the functional information into anatomical space. This step is necessary because the images in the fMRI time series typically have low spatial resolution and tissue contrast owing to a trade-off for high temporal resolution and T_2*-contrast. Co-registration importantly allows researchers to anatomically localize the patterns of brain activation that are captured in the fMRI time series. Next, similar to the structural analyses above, a spatial normalization procedure is used in which all images are warped to a standard space/template to overcome individual variability in brain shape and size to

allow for valid between-subject and group analyses. Finally, to ensure reliable spatial and temporal information in the fMRI dataset, two corresponding types of image 'smoothing' are applied. Spatial smoothing/filtering will increase the signal-to-noise ratio (SNR) and reduce effects of imperfect spatial normalizations through a procedure in which each voxel is replaced by a weighted average of neighbouring intensities (softening the edges of voxels and effectively sacrificing spatial resolution). Next, temporal smoothing/filtering is applied because the fMRI time series contain scanner-related and physiological high frequency noise that we do not need since rs-fMRI relies on low-frequency oscillations (~0.01 Hertz). The unnecessary frequencies (noise) are filtered out to leave the frequencies of interest.

1.5 Magnetic Resonance Imaging Data Analysis

1.5.1 Structural Connectivity Data Analysis

Structural MRI data including DTI and MWI can be analyzed using two common methods: whole-brain voxel-wise and ROI analyses. In voxel-wise analyses, the entire 3D brain image is parcellated into voxels that range from one to several cubic millimeters in size (e.g., 3 mm x 3 mm x 3 mm = 27 mm^3) where structural imaging values, (e.g., FA, MD and MWF), can be assessed and compared across participants at the voxel-level. Studies that use the whole-brain voxel-wise approach are often exploratory.

In the current project, however, I used an ROI approach to analyze my structural data so that I could test hypotheses about the given network node regions. In ROI-based analyses, pre-defined 3D brain volumes or ROIs (e.g., left precuneus and right caudate nucleus, or some white matter pathway) are applied to subject data, such as FA, MD, or MWF subject maps in order to extract an average FA, MD, or MWF value from all of the voxels within each ROI. The average

value that is extracted from the subject maps using the ROI is representative of the SC strength of the targeted brain region. ROIs can be defined on the basis of structural or functional information, wherein structure can be defined anatomically or using more fine-grained cytoarchitectonic classifications and function is defined using functional-MRI data. Studies that utilize the ROI approach are often hypothesis-driven because researchers can define an area or set of areas in the brain in an *a priori* manner, therefore requiring them to make predictions about those regions. Moreover, ROI analyses are good for investigating large-scale or global white matter changes in group or between-subject analyses. By allowing us to test hypotheses and conduct group analyses, the ROI approach was the most reasonable way to analyze our structural data so that we could make predictions of the corresponding functional data.

1.5.2 Functional Connectivity Data Analysis

Rs-fMRI data can be analyzed using two common methods: independent component analysis (ICA) and seed-based analysis (often referred to as ROI analysis as well). ICA is a whole-brain, data-driven approach that is useful for exploratory studies. It will extract consistent patterns of temporally coherent neural activity across the rs-fMRI time series from discrete groups of anatomically-distinct brain regions that are referred to as large-scale, resting state functional networks or intrinsic connectivity networks (Smith et al., 2013). For the purposes of this study however, a seed-based or ROI analysis was utilized, so that in similar fashion to the structural data, we would be able to test hypotheses by defining ROIs or seeds in an *a priori* manner. Wherein the SC ROI-based analysis simply extracts 3D spatial information from each ROI when applied to a structural subject map, the FC ROI-based analysis extracts four-dimensional (4D) information in that it extracts 3D spatial information over the temporal

dimension. In an FC study that applies an ROI-based analysis, FC is defined as the temporal coherence of neural activity between the selected ROIs or seeds.

Although there are numerous ways to quantify temporal coherence of an rs-fMRI time series, I will focus on one of the most accepted methods, referred to as the 'bivariate correlation' that is applied in the current project. It is a "simultaneous analysis" that produces a value with a magnitude and direction that indicates how strong the association is between two variables (Mai et al., 2005). In seed-based FC analyses, the two variables are the strengths of the MR signal from pairs of predefined-seeds over the scan duration. Strong FC between two brain regions or seeds is indicated by a high and positive bivariate correlation.

1.5.3 Magnetic Resonance Imaging Brain Atlases

In order to define an ROI or group thereof, a researcher needs an atlas that provides such coordinates within a normalized or stereotaxic brain space. There are both structurally- and functionally-defined brain atlases, and either can be applied to both structural and functional MRI data. Structurally-defined atlases are based on anatomical segmentation of white and grey matter structures, and for example may include the left and right superior frontal lobe and the left and right caudate. Functionally-defined atlases are based on functionally-connected brain regions that have been identified as part of a distinct functional network. Since the purpose of this project was to examine the relationships between structural and functional connectivity within several functional networks, I used functionally-defined atlases to analyze both my structural and functional MRI data.

Although functionally-defined atlases are common for examining rs-fMRI data, they are not as common for the analysis of structural data. In fact, previous work from our group includes a

novel publication: the UManitoba-JHU Functionally-Defined Probabilistic Human White Matter Atlas (T D Figley et al., 2015). It is the first that we know of to provide functionally-defined maps of the structural connections or white matter pathways found between functionally-connected brain regions or nodes of several well-established resting state human brain networks, including the dorsal and ventral default mode (dDMN, vDMN), the left and right executive control (lECN, rECN), and the anterior and posterior salience networks (aSN, pSN). It is based on 32 neurologically-healthy adult subjects, half male and half female. The functionally-defined white matter pathways that it outlines were identified using DTI tractography as guided in an *a priori* fashion by previously-published functionally-defined ROIs of the aforementioned networks from the Stanford fMRI Atlases (Shirer et al., 2012). Within the Stanford fMRI Atlases there are 90 functional-ROIs (fROIs) or network nodes that represent anatomically-distinct regions in the brain with FC: 9 nodes in the dDMN (36 ROI-to-ROI combinations), 10 nodes in the vDMN (45 ROI-to-ROI combinations), 6 nodes in the lECN (15 ROI-to-ROI combinations), 6 nodes in the rECN (15 ROI-to-ROI combinations), 7 nodes in the aSN (21 ROI-to-ROI combinations), and 12 nodes in the pSN (66 ROI-to-ROI combinations). These are resting state functional networks that were identified using an ICA to decode the respective subject-driven cognitive-states (Shirer et al., 2012).

Therefore, to create the UManitoba-JHU functionally-defined structural atlas, a total of 198 ROI-to-ROI contingencies were investigated across 32 subjects. Only the contingencies in which eight or more subjects demonstrated structural connectivity were used to create the group probability maps of each individual tract upon which the functionally-defined structural ROIs are based. Overall, a total of 53/198 ROI-to-ROI contingencies from the Stanford fMRI Atlas yielded robust structural connections across the six networks that were published as ROIs in the

UManitoba-JHU Atlases. There were 11 functionally-defined structural connections identified in the dDMN, 8 in the vDMN, 6 in the lECN, 6 in the rECN, 9 in the aSN and 11 in the pSN. It is across these 53 functionally-defined structural connections, within each network individually, that we conducted SC-FC relationship analyses.

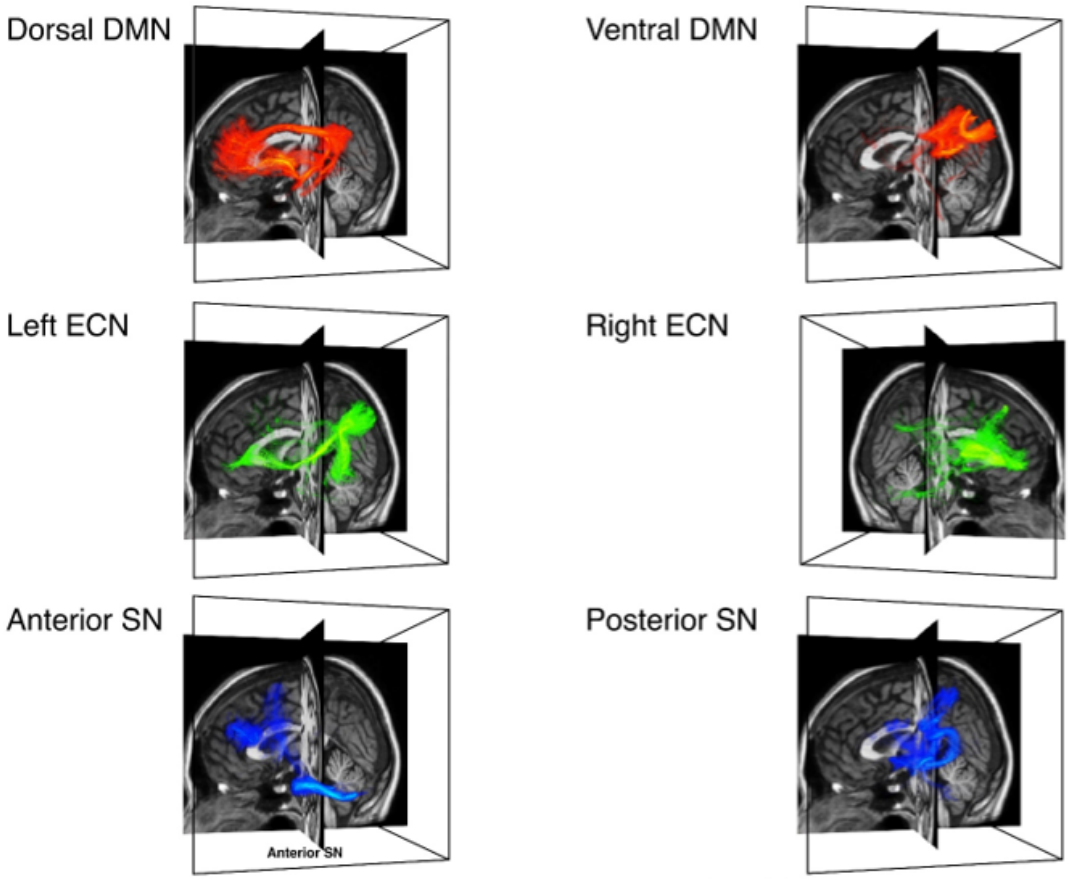

Figure 1: The Functionally-Defined Structural Connections of the Six Resting State Networks from the UManitoba-JHU Functionally-Defined Human White Matter Atlas

The fact that the tractography performed in the creation of the functionally-defined structural atlases (T D Figley et al., 2015) did not reveal robust structural connections for every pair of functionally-connected nodes (ROI-to-ROI contingencies) is a common finding in MRI studies (Damoiseaux & Greicius, 2009; Honey et al., 2009) and arises either because: 1) our current

technology cannot resolve more intricate white matter pathways, thus we simply cannot 'see' the SC, or 2) there is some indirect SC that mediates the FC.

By applying the UManitoba-JHU functionally-defined structural atlases to structural MRI data, one can extract the SC strength from each ROI that represents the white matter tracts that connect the network nodes of the aforementioned networks. Then, by applying the Stanford fMRI atlases to rs-fMRI data, one can extract the FC strength from each corresponding ROI-to-ROI contingency for which there is a structural connection as identified in the UManitoba-JHU atlases. Therefore, using these as complementary atlases with structural and functional MRI data from the same group of subjects, one can extract SC and FC strength from each network connection and make comparisons.

Chapter 2: Rationale and Objective

2.1 Problem Statement

The purpose of this thesis is to contribute to the understanding of how the structural connectivity (SC) of the brain supports functional connectivity (FC) within common resting state functional brain networks. It is important to investigate SC-FC coupling within these FC networks and to provide validation across multiple imaging modalities.

2.2 Rationale and Aims

Rationale: Previous studies that have aimed to delineate SC-FC coupling within the human brain have generally converged on the notion that SC strength between two brain regions is a reliable predictor of FC strength between those same regions, but that FC does not reliably predict SC as there are common cases of pairs of brain regions with FC but no SC. The majority of these studies rely on anatomical parcellations of the brain and exploratory whole-brain approaches that, although convenient, do not take into account well-established factors of brain organization such as distributed large-scale functional networks. Moreover, they are largely limited to diffusion-based SC metrics.

Aim: This study aims to examine how SC strength (as measured using mean diffusivity, fractional anisotropy and the myelin water fraction) correlates with FC strength (as measured using a bivariate correlation based on resting state functional magnetic resonance imaging) within the network connections of several well-established resting state networks. This work will expand our understanding of how SC couples with FC to support the various sensory, cognitive and behavioural tasks associated with healthy resting state networks.

2.3 Hypotheses

This thesis will test two distinct hypotheses: 1) that direct SC-FC relationships within each network are strong, positive, and significant (i.e., for SC and FC between the same network nodes), and 2) that indirect relationships within each network are relatively weak and insignificant (i.e., for SC and FC between partial- or non-overlapping network nodes).

Chapter 3: Manuscript

Relationships between white matter microstructure and functional connectivity throughout macroscale human brain networks

Under Review at *NeuroImage*

Abstract

It is widely presumed that functional connectivity (FC) within large-scale human brain networks is supported by the underlying white matter structural connectivity (SC). Prior studies suggest that SC strength predicts both the existence and degree of FC between anatomically-defined brain regions, but few have systematically tested how SC couples with FC throughout large-scale networks, and even fewer have employed quantitative techniques other than diffusion-based MRI to characterize SC. In the current study, we used whole-brain functional and structural MRI data from 32 neurologically-healthy adults; where resting state fMRI was used to quantify FC strength between pairs of predefined network nodes, and fractional anisotropy, mean diffusivity and myelin water fraction were used to quantify SC strength in the corresponding white matter connections between nodes within the dorsal and ventral default mode, left and right executive control, and anterior and posterior salience networks. We assessed SC-FC relationships using linear correlation and regression analyses, which revealed low direct correspondence between SC and FC strength. However, we found significant indirect SC-FC coupling wherein SC strength for a given connection was associated with FC strength from partially-overlapping (i.e., sharing one node) and non-overlapping (i.e., sharing zero nodes) connections within the same network. Moreover, we found that when at least two nodes in an SC-FC comparison were located in a rich club region, there was a greater probability that the relationship was significant. Overall, we demonstrate that structural networks indirectly support a variety of divergent functional networks through the rich club configuration.

Keywords: Structural connectivity, functional connectivity, rich club connectivity, large-scale networks

1.0 INTRODUCTION

The spectrum of sensory, motor, and cognitive processing performed in the human brain relies on the intricate wiring (structural connectivity; SC) and communication (functional connectivity; FC) between large-scale populations of nerve cells (Bressler & Menon, 2010). SC strength encompasses both the locations and physical characteristics of anatomical white matter tracts that transmit electrochemical signals between regions, and appears to have a hierarchy of network organization (Hagmann et al., 2008; van den Heuvel et al., 2012). Emerging from this SC, FC strength can be inferred through patterns of temporally correlated neural activity that is organized into various distributed large-scale networks composed of multiple anatomically-distinct brain regions (Hermundstad et al., 2013; Shirer et al., 2012).

It is known that coherent FC emerges from underlying SC, but the complex relationships through which SC supports FC is an essential and largely unknown topic (Damoiseaux & Greicius, 2009; Honey et al., 2010; Park & Friston, 2013). Initial SC-FC coupling investigations were largely qualitative: they established the presence/absence and number of fiber tracts between functionally-connected brain regions – either within a few specific connections (Greicius et al., 2009; van den Heuvel et al., 2009; van den Heuvel et al., 2008) or across the entire brain (Hagmann et al., 2008; Honey et al., 2009; Skudlarski et al., 2008). More recently, quantitative measures such as diffusion-based fractional anisotropy (FA) or edge weight have been used to predict FC strength and vice versa (Huang & Ding, 2016; Khalsa et al., 2014; Meier et al., 2016). The findings from these studies have generally converged on the notion that the strength of direct SC accurately predicts both the existence and strength of FC between two brain regions, but that direct FC does not as reliably predict SC, suggesting that indirect structural connections factor into FC and SC-FC coupling.

However, the majority of previous studies have used exploratory analyses (e.g., linear correlations, graph theoretical methods) to search for SC-FC relationships throughout a set of anatomically-defined brain regions in an approach that does not take into account critical features of functional network brain organization (Buckner et al., 2008; Seeley et al., 2007). Although a few studies have examined SC-FC coupling in brain regions associated with functional networks (Greicius et al., 2009; Huang & Ding, 2016; Khalsa et al., 2014; Mišić et al., 2016), each have used anatomical (as opposed to functional) brain parcellations. Therefore, to the best of our knowledge, no previous studies have systematically examined SC-FC coupling between functionally-defined nodes within large-scale brain networks; nor have previous studies used multimodal SC metrics – e.g., by combining diffusion measures with myelin water imaging (MWI)-based estimates of myelin water fraction (MWF; Alonso-Ortiz et al., 2015; Prasloski et al., 2012) – that might provide convergent evidence about such SC-FC relationships.

Accordingly, the aims of the current study were to apply resting state fMRI to quantify FC strength between pairs of predefined network nodes using fMRI atlases of the dorsal and ventral default mode (dDMN, vDMN), left and right executive control (lECN, rECN) and anterior and posterior salience networks (aSN, pSN; Shirer et al., 2012). Then in parallel, use FA, mean diffusivity (MD) and MWF to quantify SC strength in the white matter pathways between the same nodes using the recently published UManitoba-JHU Functionally-Defined Human White Matter Atlas of the same networks (Figley et al., 2015, 2017). We hypothesized that: 1) direct SC-FC relationships within each network would be strong, positive and significant (i.e., for SC and FC strength between the same pairs of network nodes), and 2) indirect SC-FC relationships within each network would be weak and insignificant (i.e., for SC and FC strength between partially-overlapping connections that share one node and for non-overlapping connections that

share zero nodes). We tested these hypotheses using two approaches: 1) individual analyses by testing MDxFC, FAxFC and MWFxFC correlations, and 2) collective analyses by testing how MD, FA and MWF combine to predict FC using multiple regressions.

Our findings provide convergent evidence to a recent study by Mišic and colleagues that found similar results in a whole-brain network analysis of SC-FC relationships (Mišić et al., 2016). Together, these studies present a different view of SC-FC coupling, where: 1) global measures of SC strength between regions do not appear to support low frequency, resting state FC strength between those same regions; 2) SC between regions may, in fact, facilitate FC between other pairs of partially-overlapping or non-overlapping brain regions within the same large-scale network; and 3) SC-FC relationships appear to be largely shaped by rich club connectivity.

2.0 MATERIALS and METHODS

2.1 Data Acquisition

As a part of a previous project (Figley et al., 2016), high-resolution structural and functional MRI data was acquired from 32 neurologically-healthy adults (16 male/16 female; age = 29.9 ± 10.7 years) who volunteered through a recruitment program in Baltimore, Maryland. These participants were verbally screened to exclude participants with neurological abnormalities, psychiatric disorders, or any history of substance abuse (including alcohol or tobacco). This study was approved by the Johns Hopkins University (JHU) Institutional Review Board, and all participants provided written informed consent prior to enrollment.

Both the structural and functional MRI data were acquired at the F.M. Kirby Research Center for Functional Brain Imaging, using a whole-body 3T Philips Achieva System and a 32-

channel receive-only head coil (Philips Healthcare, Best, The Netherlands). T_1-weighted, T_2-weighted, and T_2-FLAIR scans were acquired for each participant and were assessed by a board-certified radiologist to confirm the absence of structural abnormalities or other incidental findings.

2.1.2 Structural Connectivity

For each participant, diffusion tensor imaging (DTI) data were acquired using a single-shot spin echo, echo-planar imaging (SE-EPI) pulse sequence (Farrell et al., 2007): 30 diffusion-encoded images (b = 700 s/mm^2); 5 reference images (b = 0 s/mm^2); TR = 6904 ms; TE = 69 ms; Flip Angle = 90°; SENSE Factor (AP/RL) = 2.5 (2.5/1.0); FOV (AP × FH × RL) = 212 mm × 154 mm × 212 mm; Number of Transverse Slices = 70 (no inter-slice gap); Spatial Resolution (Acquired) = 2.20 mm × 2.20 mm × 2.20 mm; Spatial Resolution (Resampled) = 0.83 mm × 0.83 mm × 2.20 mm; Scan Duration = 4 min and 16 s. Preprocessing of the DTI data included motion correction, coregistration of the diffusion-weighted images to the mean b = 0 s/mm^2 image, eddy current correction, calculation of six tensor images, a two-step (automatic, then manual) skull-stripping procedure, and spatial normalization of the diffusion-weighted and tensor images via a 12-parameter (linear affine) transformation followed by high-dimensional, non-linear warping via the Large Deformation Diffeomorphic Metric Mapping (LDDMM) algorithm (Beg et al., 2005). The normalized participant tensor images were then used to generate normalized FA and MD maps.

For each participant, MWI data were acquired using the following previously reported whole-brain multi-component T2-relaxation, 3D combined gradient and spin echo (GRASE) sequence (Prasloski et al., 2012): TR = 1500 ms; Echo Train Lengths = 32; Echo Spacing = 10.36 ms; Minimum TE = 10.36 ms; Maximum TE = 331.58 ms; Flip Angle = 90°; EPI Factor =

3 (in the z-direction); SENSE Factor (AP/RL/FH) = 4.0 (1.0/2.0/2.0); FOV (AP x RL x FH) = 212 mm x 212 mm x 96 mm; Spatial Resolution = 0.95 mm x 0.95 mm x 3.00 mm; Scan Duration = 7 min and 29 s. Preprocessing of the MWI data included coregistration of the myelin water images to a high-resolution anatomical T_1-weighted image (acquired using a 3D magnetization-prepared, rapid gradient echo [MP-RAGE] sequence), a two-step skull-stripping procedure, and normalization of the participant T_1 via a 12-parameter (linear affine) transformation then a high-dimensional, non-linear warping via the LDDMM algorithm (Beg et al., 2005) – the results of which are then applied in order to normalize the participant myelin water images. MWF maps for each participant were then calculated using a multi-exponential, non-negative least squares (NNLS) algorithm to: 1) fit the multi-exponential T2 decay from different water compartments, while 2) compensating for stimulated echoes, as previously reported (Hennig et al., 2003; Prasloski et al., 2012).

2.1.3 Functional Connectivity

For each participant, resting state fMRI data were acquired using the following whole-brain T_2^*-weighted gradient-echo, echo planar imaging (GE-EPI) pulse sequence (Choe et al., 2015): TR = 2000 ms; TE = 30 ms; Flip Angle = 70°; SENSE Factor (AP/RL) = 2.0 (1.0/2.0); FOV (AP x FH x RL) = 200 mm × 104.5 mm × 180 mm; Number of Transverse Slices = 35 (ascending acquisition with 0.50 mm inter-slice gap); Spatial Resolution = 2.50 mm × 2.50 mm × 2.50 mm; Scan Duration = 7.4 minutes; 6 unused "steady-state" volumes followed by 216 resting state fMRI volumes. Participants were asked to fixate on a white central cue that was projected onto a screen outside the scanner and made visible by a mirror mounted directly to the head coil. Preprocessing of the resting state fMRI data included slice-time correction, realignment to the mean T_2*-weighted image, coregistration to the high-resolution anatomical MP-RAGE T_1-

weighted image, spatial normalization to the ICBM152 template (Mazziotta et al., 1995) via unified segmentation (Ashburner & Friston, 2005), and three-dimensional smoothing with a 6 mm full-width half-maximum (FWHM) Gaussian kernel.

We also implemented further temporal preprocessing steps utilizing the SPM Conn Toolbox (http://www.nitrc.org/projects/conn, Massachusetts Institute of Technology, Cambridge, MA) to regress out the effects of participant motion (i.e., the six realignment parameters from rigid-body registration) and physiological motion (i.e., the time-courses of eroded white matter and cerebrospinal fluid masks using the CompCor method; Behzadi et al., 2007). We then used the Artifact Detection Tool (http://www.nitrc.org/projects/artifact_detect/, Massachusetts Institute of Technology, Cambridge, MA) to identify and regress out time-points with scan-to-scan intensity changes of $z > 3.0$, translational motion > 0.50 mm in any direction, and/or rotational motion > 0.05° in any plane. The resting state fMRI data were then temporally band-pass filtered (0.01–0.08 Hz) to isolate the low frequency fluctuations of interest (Biswal et al., 1995).

2.2 Extraction of Structural Connectivity and Functional Connectivity Metrics

We used complementary structural (UManitoba-JHU Functionally-Defined Human White Matter Atlases; Figley et al., 2015, 2017) and functional (Stanford fMRI Atlases; Shirer et al., 2012) human brain atlases to quantify SC and FC strength within the network connections of the dDMN, vDMN, lECN, rECN, aSN, and pSN. The UManitoba-JHU Functionally-Defined Human White Matter Atlases were downloaded from the NITRC website (http://www.nitrc.org/projects/uofm_jhu_atlas) and each tract was used as an ROI in order to extract FA, MD and MWF values as metrics of SC strength across all 32 participants. Then, the Stanford fMRI Atlases were downloaded from the Functional Imaging in Neuropsychiatric Disorders Lab website (http://findlab.stanford.edu/functional_ROIs.html) and each pair of

network nodes corresponding to the tracts in the UManitoba-JHU atlas were used as seeds to calculate bivariate correlations as a measure of FC strength throughout the entire resting state fMRI time series. It is important to note that the FC strength was calculated only for the functional network connections that also have corresponding structural connections as charted in the structural atlas. Therefore, for each connection analyzed across the six networks, we had three metrics of SC strength (i.e., FA, MD, and MWF) as defined by the structural atlas, and one metric of FC strength (i.e., bivariate correlation) as defined by the complementary functional atlas. The MD, FA, MWF, and FC values were standardized by calculating z-scores for each connection (i.e., across participants), which were then used for all statistical analyses.

2.3 Structural Connectivity vs. Functional Connectivity Comparisons

We examined direct SC-FC relationships by comparing the SC strength (i.e., MD, FA, and MWF) for a given network connection with FC strength (i.e., bivariate correlation) of the same connection. We then examined indirect SC-FC relationships by comparing the SC strength for a given network connection to the FC strength from all other partially-overlapping and non-overlapping connections within the same network. We used Pearson correlation analyses to assess individual linear relationships between each SC metric and FC. Correlations with $p < 0.05$ were considered significant. We then used multiple regression analyses to assess the collective power of all three SC metrics as independent variables (IVs) to predict FC values (the dependent variable [DV]). $R^2_{adjusted}$ values were used as a measure of the variance in FC strength accounted for by all three SC strength measures. Regression models were considered significant when the F-statistic produced from the ANOVA had $p < 0.05$.

Increases in both FA and MWF correspond to an increase in SC strength (Alexander et al., 2007; MacKay & Laule, 2016), whereas an increase in MD corresponds to a decrease in SC

strength (Alexander et al., 2007). Therefore, to be consistent and ease interpretation of the results, the inverse of MD was utilized in the correlation and regression analyses so that all three SC metrics indicated SC in the same direction. Also, it is well-established that neither participant-wise variations among functionally-defined connections within human brain networks nor the three SC metrics are independent (MacKay et al., 2016; Smith et al., 2013). Consequently, we did not run a multiple comparisons correction and included only uncorrected correlation and regression findings in this report.

3.0 RESULTS

3.1 Direct SC-FC Relationships

We first tested the hypothesis that direct SC-FC relationships within each network are strong, positive, and significant (e.g., SC strength from connection D1-D3 should be strongly associated with FC strength from D1-D3 in the dDMN) by means of linear correlation and then regression. In the correlational analyses, there were 11 functional connections with direct white matter tracts (as defined by the Figley et al. 2015 atlases) in the dDMN, 8 in the vDMN, 6 in the lECN, 8 in the rECN, 9 in the aSN, and 11 in the pSN, in which to test direct SC-FC relationships. The most striking feature of the uncorrected direct SC-FC correlations is that the majority were weak and insignificant across all six networks – a pattern that transcended all three SC metrics with only 2/53 (3.8%) tests for MDxFC, 2/53 (3.8%) tests for FAxFC, and 1/53 (1.9%) tests for MWFxFC having revealed positive and significant Pearson correlations at (Figures 1-3). Our correlation analyses were corroborated by the uncorrected regression models, which revealed only 1/53 (1.9%) direct SC-FC relationship models in which MD, FA and MWF as a collective measure of SC strength accounted for a significant proportion of variance in FC

strength (Figure 4). We expected to find a high rate of strong and positive direct SC-FC relationships in both the correlation and regression analyses, but instead our findings indicate that the presence of direct SC strength does not reliably predict FC strength in network-level connections within the dDMN, vDMN, lECN, rECN, aSN, and pSN.

Figure 1

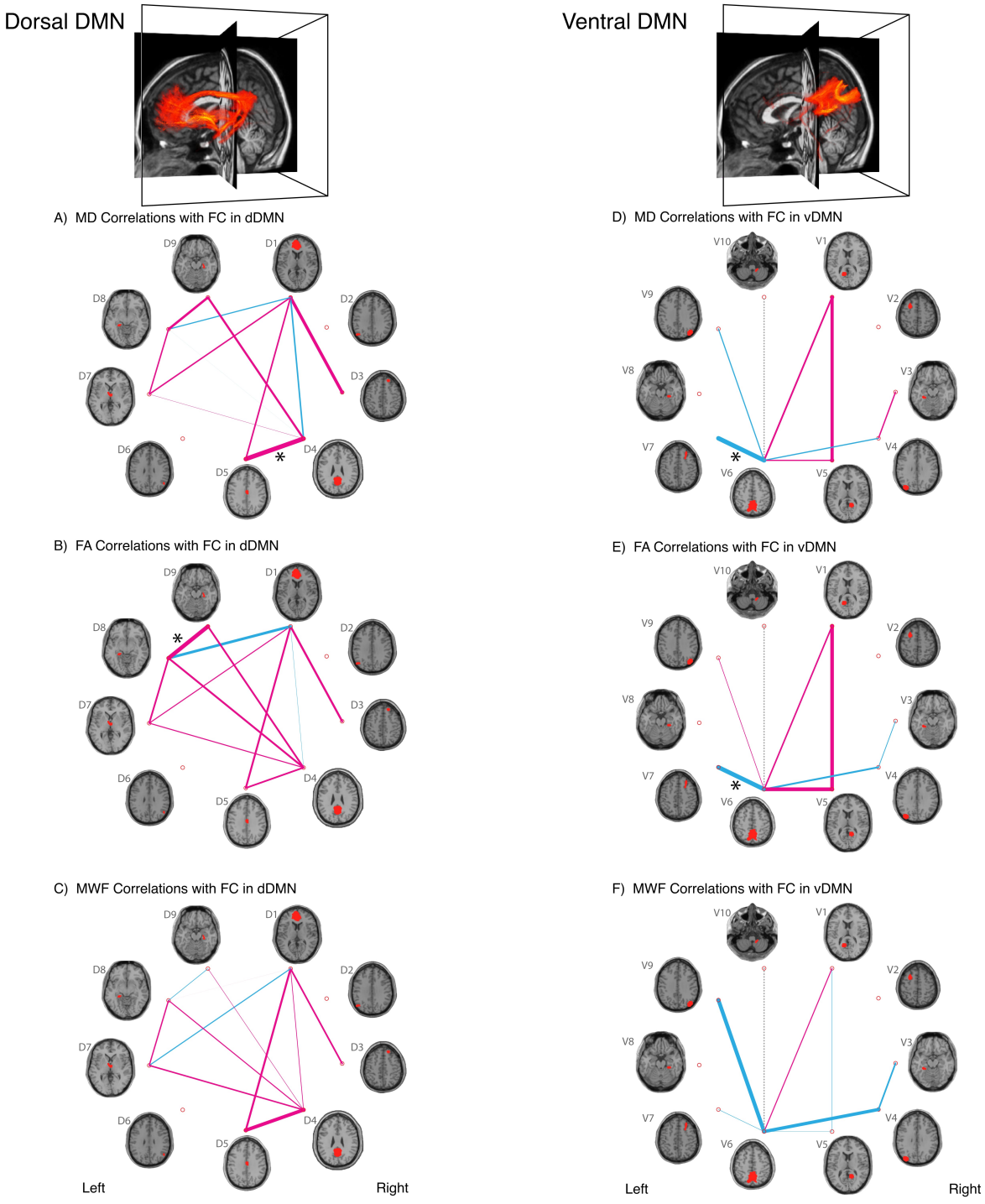
Dorsal DMN
Ventral DMN
A) MD Correlations with FC in dDMN
D) MD Correlations with FC in vDMN
B) FA Correlations with FC in dDMN
E) FA Correlations with FC in vDMN
C) MWF Correlations with FC in dDMN
F) MWF Correlations with FC in vDMN
D1
D2
D3
D4
D5
D6
D7
D8
D9
V1
V2
V3
V4
V5
V6
V7
V8
V9
V10
Left
Right

***Figure 1**: Direct Relationships between Structural Connectivity (SC) and Functional Connectivity (FC) strength in the Dorsal and Ventral Default Mode Networks (dDMN, vDMN). Axial slices depict the functional-ROIs (in red) utilized from the Stanford FC Atlases (Shirer et al. 2012) to quantify FC. The solid lines that connect each axial slice indicate the corresponding functionally-defined structural connections that were quantified using the Figley et al., (2015) atlases. The thickness of the lines indicates the magnitude of the Pearson correlation coefficient as a measure of linear dependence between the three SC metrics (Mean Diffusivity (MD), Fractional Anisotropy (FA), Myelin Water Fraction (MWF)) and FC for direct (e.g., SC from D1_D3 with FC from D1_D3) SC-FC relationships; magenta colour indicates a positive relationship; cyan colour indicates a negative relationship; significant relationships ($p<0.05$) are marked with an asterisk. The inverse of MD was used to compute correlations with FC so that an increase in MD, FA, and MWF all correspond to an increase in SC; this approach was taken in order to simplify interpretation of correlations with FC. The 3D visualization depicts the functionally-defined white matter tracts.*

Figure 2

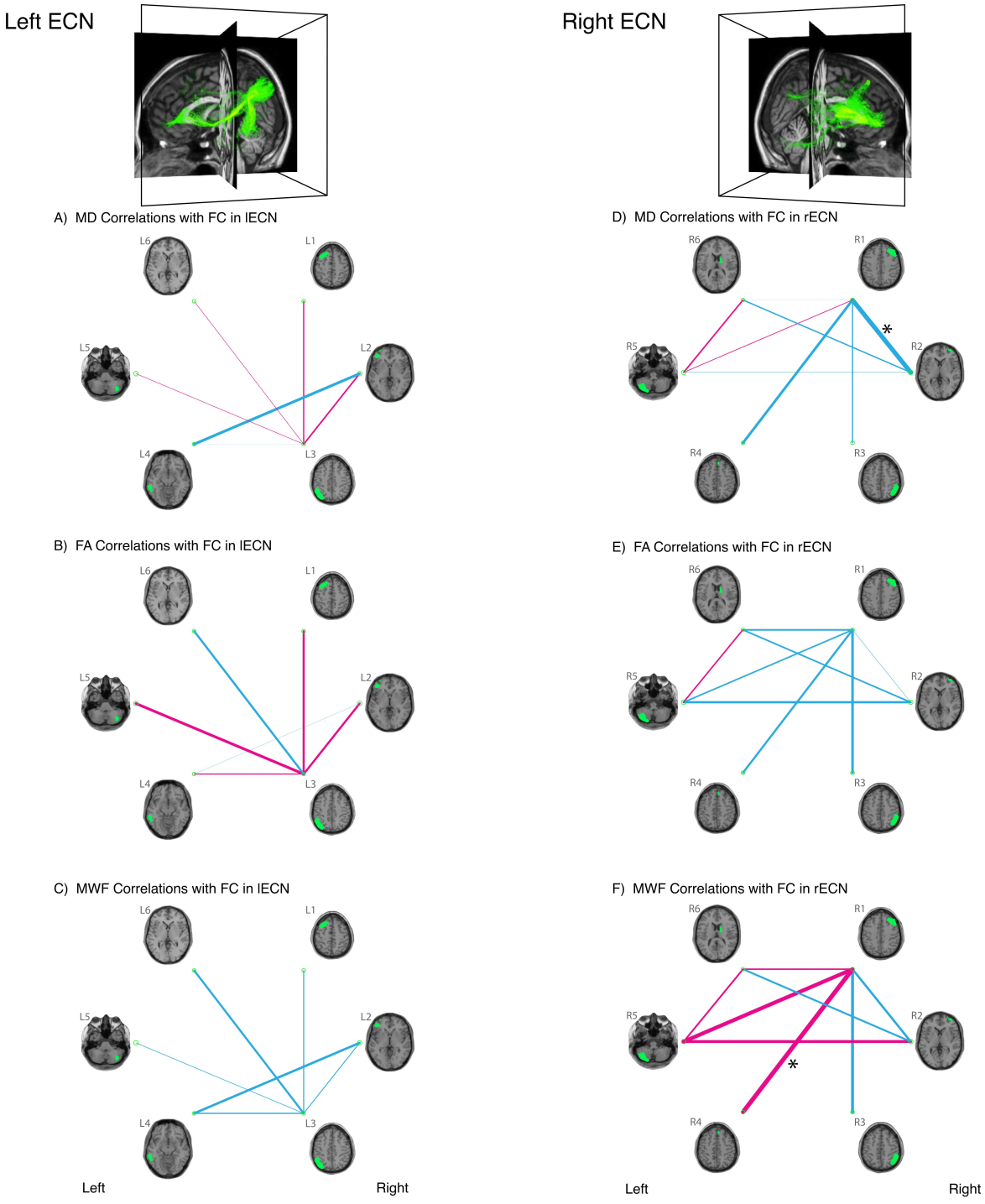
Left ECN
Right ECN
A) MD Correlations with FC in lECN
D) MD Correlations with FC in rECN
B) FA Correlations with FC in lECN
E) FA Correlations with FC in rECN
C) MWF Correlations with FC in lECN
F) MWF Correlations with FC in rECN
L6
L1
L5
L2
L4
L3
R6
R1
R5
R2
R4
R3
*
*
Left
Right
Left
Right

***Figure 2**: Direct Relationships between Structural Connectivity (SC) and Functional Connectivity (FC) strength in the Left and Right Executive Control Networks (lECN, rECN). Axial slices depict the functional-ROIs (in green) utilized from the Stanford FC Atlases (Shirer et al. 2012) to quantify FC. The solid lines that connect each axial slice indicate the corresponding functionally-defined structural connections that were quantified using the Figley et al., (2015) atlases. The thickness of the lines indicates the magnitude of the Pearson correlation coefficient as a measure of linear dependence between the three SC metrics (Mean Diffusivity (MD), Fractional Anisotropy (FA), Myelin Water Fraction (MWF)) and FC for direct (e.g., SC from L1_L3 with FC from L1_L3) SC-FC relationships; magenta colour indicates a positive relationship; cyan colour indicates a negative relationship; significant relationships ($p<0.05$) are marked with an asterisk. The inverse of MD was used to compute correlations with FC so that an increase in MD, FA, and MWF all correspond to an increase in SC; this approach was taken in order to simplify interpretation of correlations with FC. The 3D visualization depicts the functionally-defined white matter tracts.*

Figure 3

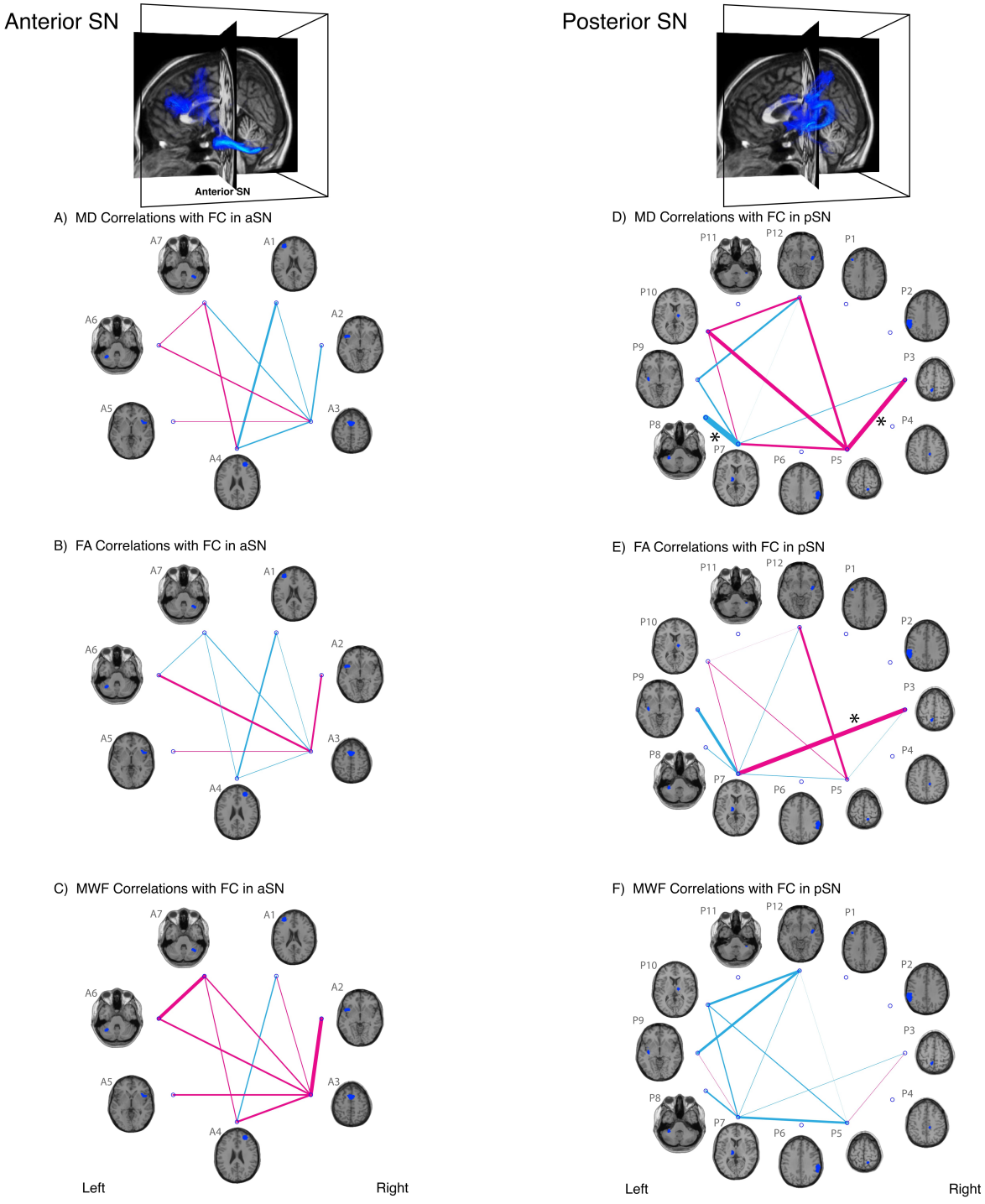
Anterior SN
Anterior SN
Posterior SN
A) MD Correlations with FC in aSN
D) MD Correlations with FC in pSN
B) FA Correlations with FC in aSN
E) FA Correlations with FC in pSN
C) MWF Correlations with FC in aSN
F) MWF Correlations with FC in pSN
A7
A1
A6
A2
A5
A3
A4
P11
P12
P1
P10
P2
P9
P3
P8
P4
P7
P6
P5
Left
Right
Left
Right

***Figure 3**: Direct Relationships between Structural Connectivity (SC) and Functional Connectivity (FC) strength in the Anterior and Posterior Salience Networks (aSN, pSN). Axial slices depict the functional-ROIs (in blue) utilized from the Stanford FC Atlases (Shirer et al. 2012) to quantify FC. The solid lines that connect each axial slice indicate the corresponding functionally-defined structural connections that were quantified using the Figley et al., (2015) atlases. The thickness of the lines indicates the magnitude of the Pearson correlation coefficient as a measure of linear dependence between the three SC metrics (Mean Diffusivity (MD), Fractional Anisotropy (FA), Myelin Water Fraction (MWF)) and FC for the direct (e.g., SC from A1_A3 with FC from A1_A3) SC-FC relationships; magenta colour indicates a positive relationship; cyan colour indicates a negative relationship; significant relationships ($p<0.05$) are marked with an asterisk. The inverse of MD was used to compute correlations with FC so that an increase in MD, FA, and MWF all correspond to an increase in SC; this approach was taken in order to simplify interpretation of correlations with FC. The 3D visualization depicts the functionally-defined white matter tracts.*

Figure 4

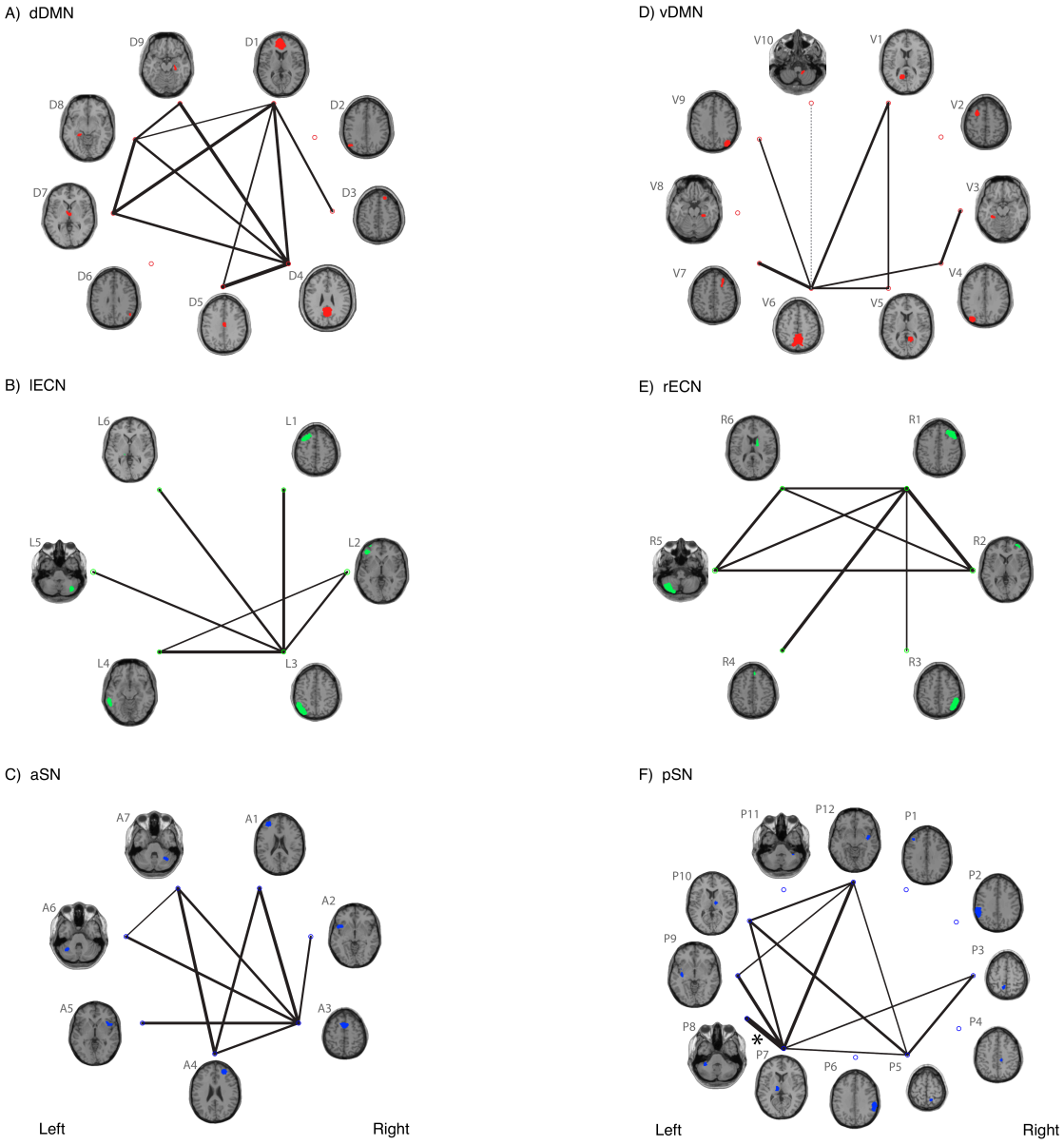

Figure 4*: Direct Relationships between Structural Connectivity (SC) and Functional Connectivity (FC) strength in the Dorsal and Ventral Default Mode Networks (dDMN, vDMN) [red ROIs], Left and Right Executive Control Networks (lECN, rECN) [green ROIs], and*

Anterior and Posterior Salience Networks (aSN, pSN) [blue ROIs] as measured using regression analyses. The solid lines that connect each axial slice indicate the corresponding functionally-defined structural connections that were quantified using the Figley et al., (2015) atlases. The thickness of the lines indicate the magnitude of the $R^2_{adjusted}$ *values for all direct SC-FC relationship regression models as a measure of how much variance the combination of the independent variables (IV) IV1=MD, IV2=FA, IV3=MWF, account for in the dependent variable (DV), FC. The inverse of MD was used in the analyses so that an increase in MD, FA, and MWF all correspond to an increase in SC; this approach was taken in order to simplify interpretation relationships with FC. SC-FC relationships in which SC accounted for a significant ($p < 0.05$) amount of variance in FC are indicated by an asterisk.*

3.2 Indirect SC-FC Relationships

We next tested the hypothesis that indirect SC-FC relationships within each network are weak and insignificant (e.g., SC strength from connection D1-D3 in the dDMN should not be strongly associated with FC strength from all other partially-overlapping or non-overlapping dDMN connections – D1_D4, D1_D6, D1_D7, D1_D8, D4_D5, D4_D7, D4_D8, D4_D9, D7_D8, D8_D9) by means of linear correlation and then multiple regression analyses. Across all six networks, there were 402 indirect SC-FC relationships to test. The most striking feature of the indirect SC-FC relationships as tested by linear correlations is that we uncovered 142 uncorrected indirect relationships with moderate correlations at $r > 0.3$ and $p < 0.1$ in seemingly non-random patterns across all three SC metrics (Figures 5-8). Although we expected no indirect correlations between SC and FC strength, we identified an indirect SC-FC pattern that transcended all three SC metrics with 30/402 (5.0%) tests for MDxFC, 20/402 (7.5%) tests for

FAxFC, and 7/402 (1.7%) tests for MWFxFC with significant correlations at $p < 0.05$ (Figures 5-8). For instance, within the dDMN, the FC strength of connection D4_D5 was positively correlated with SC strength as measured by MD in D4_D8 and D4_D9 (Figure 5A), as measured by FA in D1_D8 (Figure 5A), and as measured by MWF in D1_D4, D1_D6, D1_D8, and D7_D8 (Figure 5A). Interestingly, our correlation analyses also revealed significant negative correlations in patterns that transcended all three SC metrics. For instance, within the rECN, the FC strength of connection R1_R2 was negatively correlated with the MD values of connections R1_R5, R1_R6, and R2_R6 and the FA values of connections R1_R3 and R5_R6 (Figure 6B); the FC strength of connection R1_R2 also demonstrated trends toward significant negative correlation with the SC strength as measured by MWF in connections R1_R5, R2_R6, and R5_R6 (Figure 6B). These unexpected correlational findings were corroborated by the regression analyses, which revealed that for 18/402 (4.5%) of the indirect SC-FC relationship models, SC strength indirectly accounted for a significant proportion of variance in FC strength (Figure 8).

Therefore, although we expected to find strong and positive direct SC-FC relationships, as well as weak and insignificant indirect SC-FC relationships, our findings indicate that the presence of direct SC does not reliably predict FC strength in network-level connections within the dDMN, vDMN, lECN, rECN, aSN, and pSN, but that structural configurations can support a range of indirect functional configurations.

Figure 5

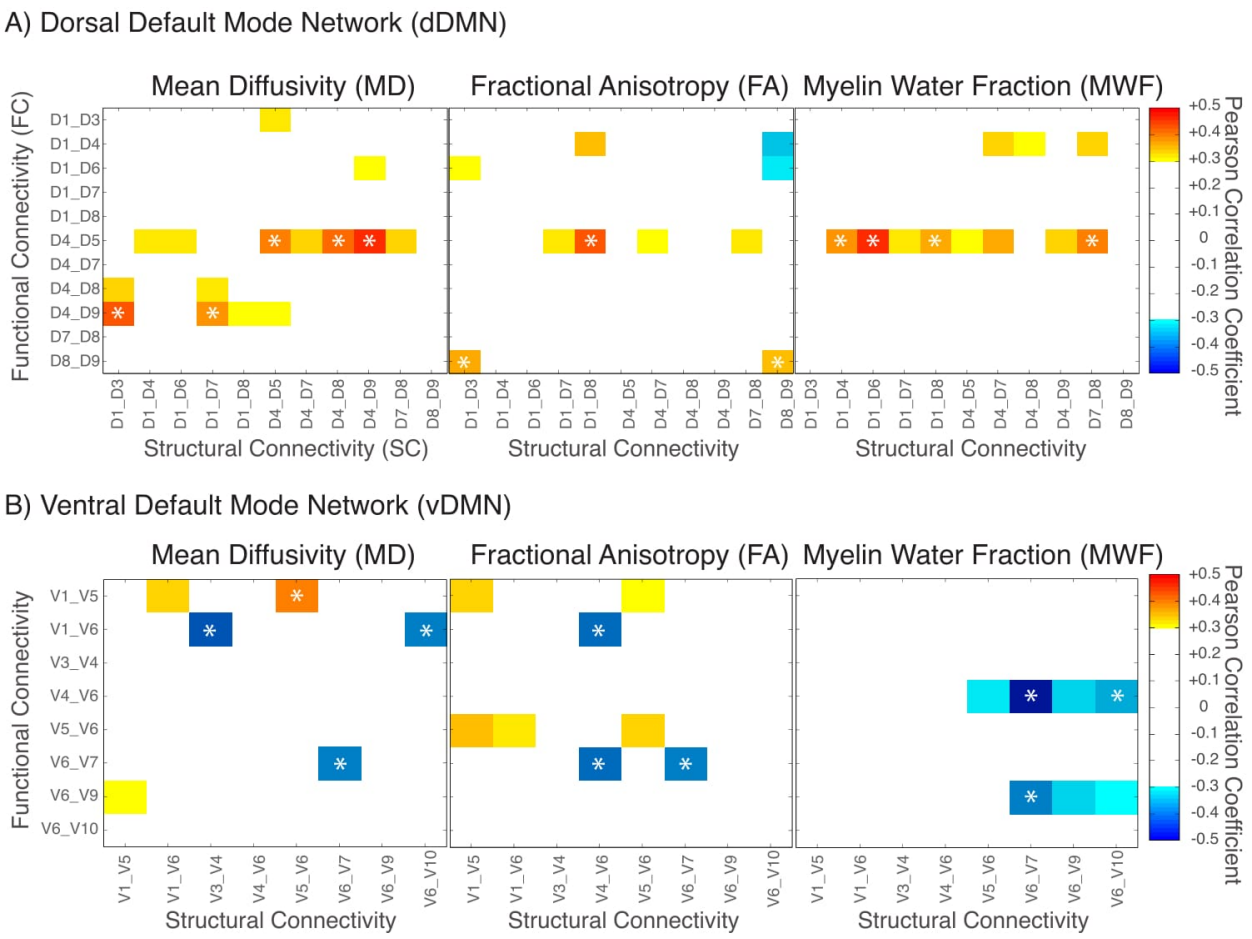

Figure 5*: Indirect Relationships between Structural Connectivity (SC) and Functional Connectivity (FC) strength in the Dorsal and Ventral Default Mode Networks (dDMN, vDMN). Colour matrices depict the magnitude and direction of the Pearson correlation coefficient (r) as a measure of linear dependence between the three SC metrics (Mean Diffusivity (MD), Fractional Anisotropy (FA), Myelin Water Fraction (MWF)) and FC for both direct (e.g., SC from D1_D3 with FC from D1_D3) and indirect (e.g., SC from D1_D3 with FC from D1_D4) SC-FC relationships. The inverse of MD was used to compute correlations with FC so that an increase in MD, FA, and MWF all correspond to an increase in SC; this approach was taken in order to simplify interpretation of correlations with FC. A colour map threshold at p<0.10 (i.e., -*

30 ≥ r ≤ 0.30) was applied to distinguish SC-FC connection combinations that trend toward strong relationships; significant relationships (p < 0.05) are marked with an asterisk.

Figure 6

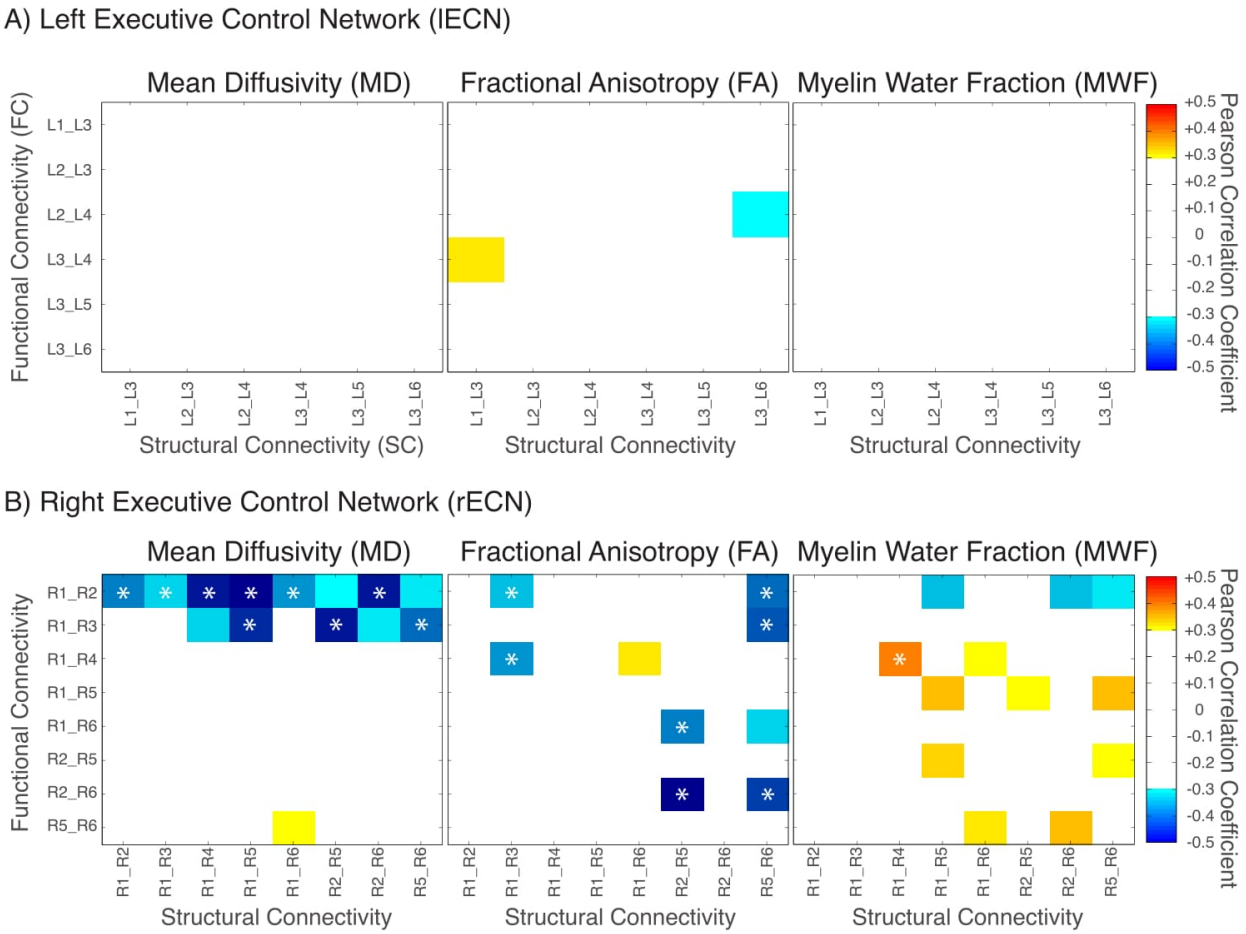

Figure 6*: Indirect Relationships between Structural Connectivity (SC) and Functional Connectivity (FC) strength in the Left and Right Executive Control Networks (lECN, rECN). Colour matrices depict the magnitude and direction of the Pearson correlation coefficient (r) as a measure of linear dependence between the three SC metrics (Mean Diffusivity (MD), Fractional Anisotropy (FA), Myelin Water Fraction (MWF)) and FC for both direct (e.g., SC from L1_L3 with FC from L1_L3) and indirect (e.g., SC from L1_L3 with FC from L2_L3) SC-*

FC relationships. The inverse of MD was used to compute correlations with FC so that an increase in MD, FA, and MWF all correspond to an increase in SC; this approach was taken in order to simplify interpretation of correlations with FC. A colour map threshold at p<0.10 (i.e., -30 ≥ r ≤ 0.30) was applied to distinguish SC-FC connection combinations that trend toward strong relationships; significant relationships (p < 0.05) are marked with an asterisk.

Figure 7

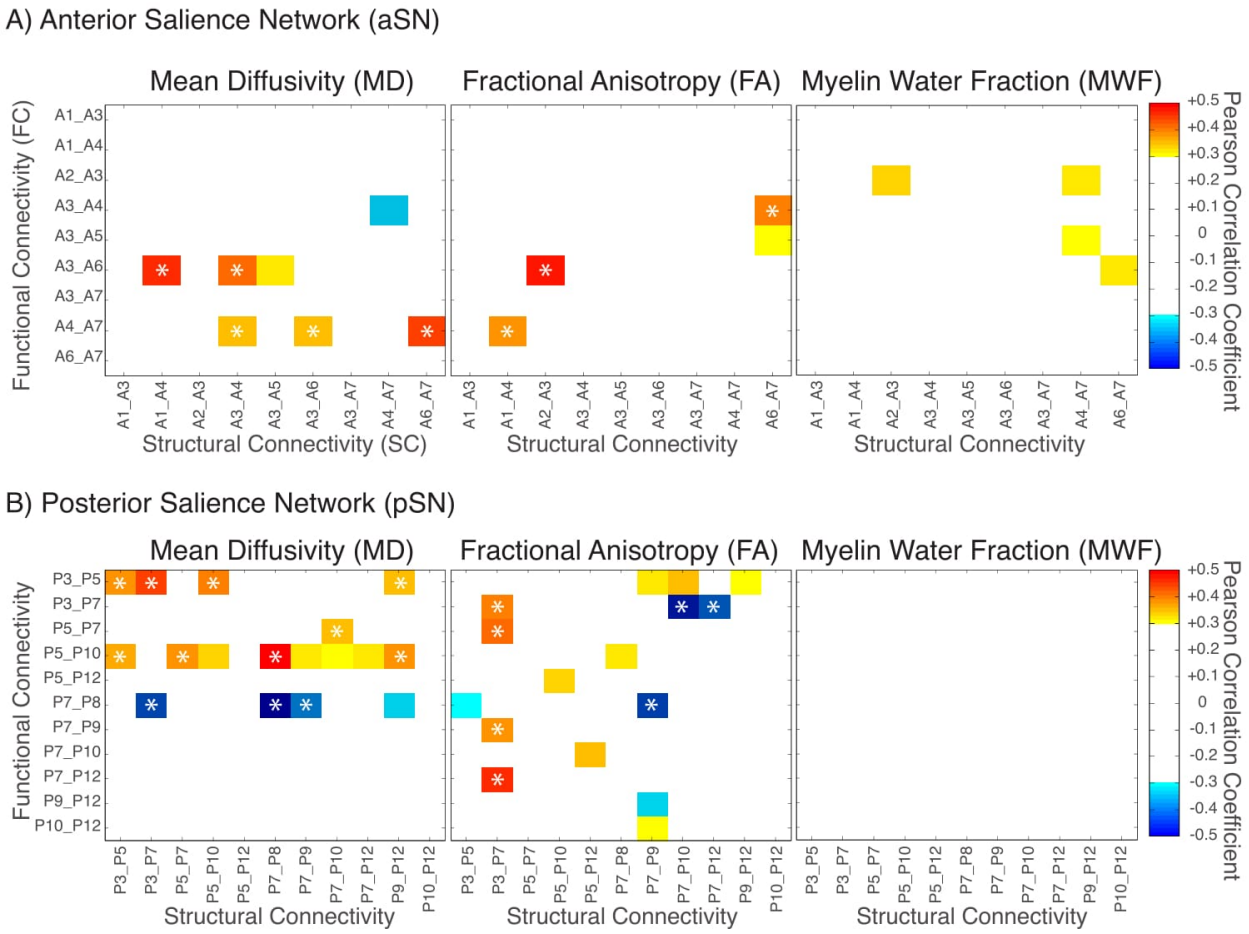

Figure 7*: Indirect Relationships between Structural Connectivity (SC) and Functional Connectivity (FC) strength in the Anterior and Posterior Salience Networks (aSN, pSN). Colour matrices depict the magnitude and direction of the Pearson correlation coefficient as a measure*

of linear dependence between the three SC metrics (Mean Diffusivity (MD), Fractional Anisotropy (FA), Myelin Water Fraction (MWF)) and FC for both direct (e.g., SC from A1_A3 with FC from A1_A3) and indirect (e.g., SC from A1_A3 with FC from A1_A4) SC-FC relationships. The inverse of MD was used to compute correlations with FC so that an increase in MD, FA, and MWF all correspond to an increase in SC; this approach was taken in order to simplify interpretation of correlations with FC. A colour map threshold at $p<0.10$ (i.e., $-30 \geq r \leq 0.30$) was applied to distinguish SC-FC connection combinations that trend toward strong relationships; significant relationships ($p < 0.05$) are marked with an asterisk.

Figure 8

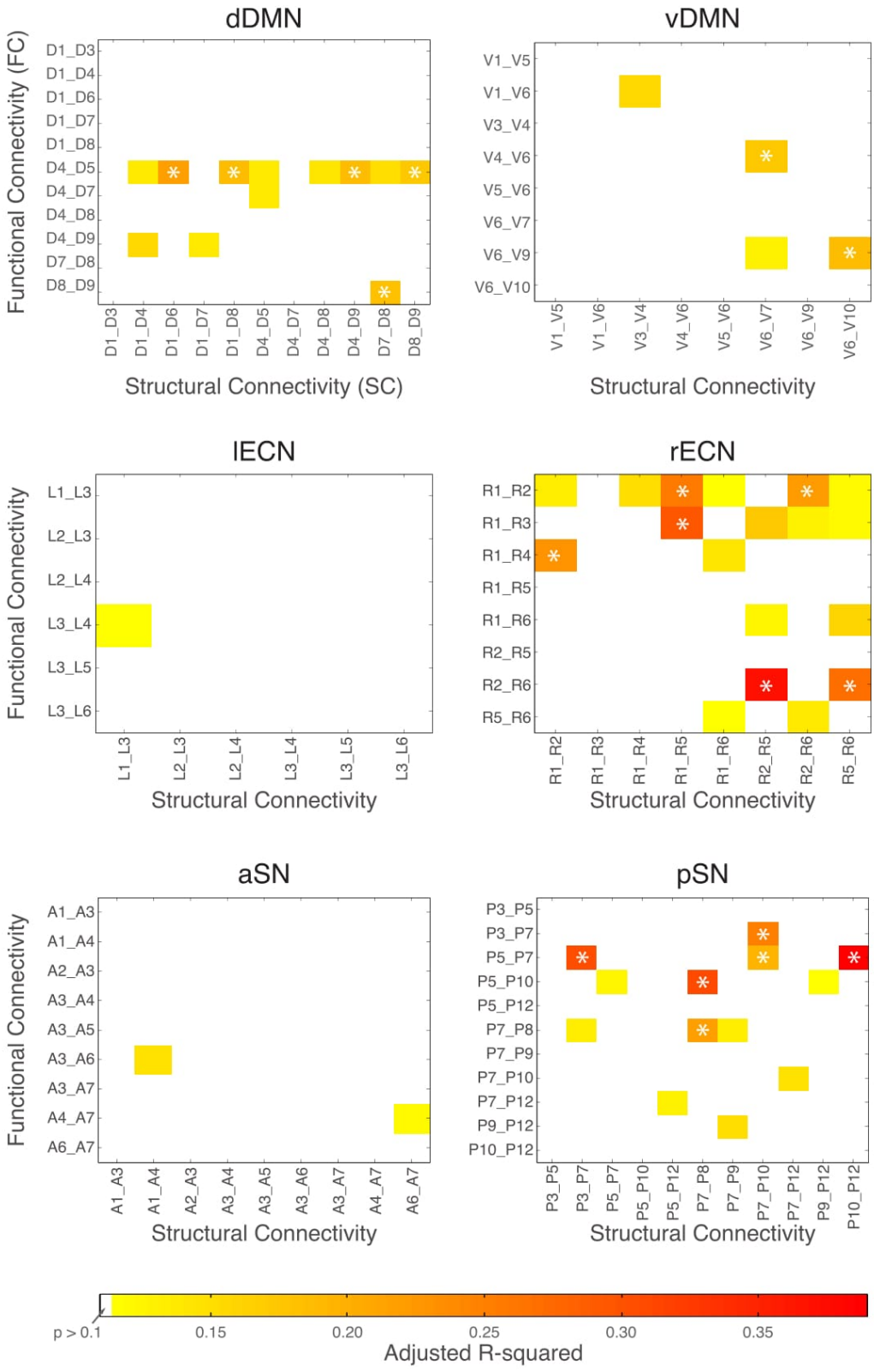
dDMN
Functional Connectivity (FC)
D1_D3
D1_D4
D1_D6
D1_D7
D1_D8
D4_D5
D4_D7
D4_D8
D4_D9
D7_D8
D8_D9
Structural Connectivity (SC)
vDMN
V1_V5
V1_V6
V3_V4
V4_V6
V5_V6
V6_V7
V6_V9
V6_V10
Structural Connectivity
lECN
Functional Connectivity
L1_L3
L2_L3
L2_L4
L3_L4
L3_L5
L3_L6
Structural Connectivity
rECN
R1_R2
R1_R3
R1_R4
R1_R5
R1_R6
R2_R5
R2_R6
R5_R6
Structural Connectivity
aSN
Functional Connectivity
A1_A3
A1_A4
A2_A3
A3_A4
A3_A5
A3_A6
A3_A7
A4_A7
A6_A7
Structural Connectivity
pSN
P3_P5
P3_P7
P5_P7
P5_P10
P5_P12
P7_P8
P7_P9
P7_P10
P7_P12
P9_P12
P10_P12
Structural Connectivity
p > 0.1
0.15
0.20
0.25
0.30
0.35
Adjusted R-squared

***Figure 8**: Indirect Relationships between Structural Connectivity (SC) and Functional Connectivity (FC) strength in the Dorsal and Ventral Default Mode Networks (dDMN, vDMN), Left and Right Executive Control Networks (lECN, rECN), and Anterior and Posterior Salience Networks (aSN, pSN). Colour matrices depict the magnitude of the $R^2_{adjusted}$ values for all SC-FC relationship regression models as a measure of how much variance the combination of the independent variables (IV) IV1=MD, IV2=FA, IV3=MWF, account for in the dependent variable (DV), FC. The inverse of MD was used in the analyses so that an increase in MD, FA, and MWF all correspond to an increase in SC; this approach was taken in order to simplify interpretation relationships with FC. The lower-bound of the colour map was chosen as $R^2_{adjusted} = 0.115$ which in the ANOVA test for the model corresponded to an F statistic with $p < 0.10$, in order to distinguish SC-FC relationships that trended toward significance. The upper-bound was the highest identified $R^2_{adjusted}$ value, 0.39. The cut-off for model significance at $p<0.05$ corresponded approximately to an $R^2_{adjusted} = 0.177$, as indicated on the colour bar. SC-FC relationships in which SC accounted for a significant ($p < 0.05$) amount of variance in FC are indicated by an asterisk.*

3.3 Rich Club Participation in SC-FC Relationships

Lastly, we also conducted post-hoc analyses in order to characterize the involvement of rich club brain regions (van den Heuvel et al., 2012; van den Heuvel & Sporns, 2011) among the significant SC-FC relationships within each network. We refer to network nodes located in rich club regions as 'rich club nodes' and those located in non-rich club regions as 'non-rich club nodes'. For each SC-FC combination, there are four nodes involved (i.e., two from which SC strength is derived and two from which FC strength is derived), of which zero-to-four could be

rich club nodes. By counting every combination of nodes in the direct and indirect SC-FC comparisons within all six networks, we found that nearly all (63/66 = 95.5%) of the significant SC-FC relationships from our correlational analyses (Figures 5-7) and the majority (12/19 = 63%) of significant models from our regression analyses (Figure 8) included two or more rich club nodes. Moreover, SC-FC combinations with two or more rich club nodes were nearly twice as likely (14%) to have a significant relationship in the correlational analyses (Figures 5-7) relative to SC-FC combinations with only one or zero rich club nodes (8%). Therefore, our findings indicate a disproportionate involvement of rich club nodes in SC-FC relationships.

4.0 DISCUSSION

In the present study, we provide evidence for indirect and divergent SC-FC coupling within six large-scale functional networks in the human brain, including the dDMN, vDMN, lECN, rECN, aSN, and pSN. What we introduced in this report is, to the best of our knowledge, the first *a priori* test of SC-FC relationships using strictly functionally-defined brain regions to quantify both SC and FC. Notably, our analyses identified a lack of direct SC-FC correspondence within the connections of these networks; instead revealing that SC configurations support partially-overlapping and non-overlapping FC patterns through indirect connections within large-scale networks which appear to be predominately facilitated by rich club brain regions.

4.1 Divergent Relationships between Structural Connectivity and Functional Connectivity

Our findings challenge the notion that the strength of direct SC reliably predicts the strength of FC – at least within large-scale brain networks – and extend our understanding about how indirect SC-FC coupling occurs within the human brain (Greicius et al., 2009; Hagmann et al., 2008; Hermundstad et al., 2013, 2014; Honey et al., 2009; Koch et al., 2002; van den Heuvel et

al., 2008). We found that within large-scale functional network connections, SC between regions does not appear to directly support low frequency, resting state FC between those same regions, but instead that SC may, in fact, facilitate FC between other pairs of partially-overlapping or non-overlapping brain regions within the same network. Despite our deviation from the idea that the degree of direct SC predicts FC strength (Damoiseaux & Greicius, 2009; Honey et al., 2010), the concept of indirect or divergent SC-FC coupling is reinforced by studies which found that FC patterns: 1) often exist despite the absence of directly corresponding SC, and 2) sometimes even diverge from the underlying SC (Greicius et al., 2009; Hagmann et al., 2008; Honey et al., 2009). Interestingly, computational studies that model the coherence of simulated brain activity based on structural networks in both animals (Deco et al., 2011; Honey et al., 2007) and humans (Deco et al., 2012, 2013; Honey et al., 2009; Rubinov & Sporns, 2010; Stam et al., 2016) have also suggested that indirect SC could account for partially-overlapping and/or non-overlapping FC patterns found at the network level (Park & Friston, 2013). Therefore, taken together, these modeling studies along with our empirical findings demonstrate that large-scale SC configurations are not only capable of supporting a diverse range of indirect FC configurations, but that this is likely borne out in reality.

Moreover, our results converge with those of another recent study by Mišić et al. (2016), which applied an exploratory whole-brain, anatomical-parcellation approach to examine SC-FC coupling within several functional networks and found that SC strength indirectly predicts FC strength at the whole-network level. We extend that conclusion to the level of individual network connections by showing strong indirect associations between different connections within multiple large-scale functional networks, where: 1) single structural connections appear to support multiple partially-overlapping and/or non-overlapping functional connections, and 2)

single functional connections may be indirectly supported by numerous structural connections. Moreover, the consistency that we identified across multimodal SC metrics provides convergent evidence that speaks to the validity of the relationships identified.

However, it is worth noting that our findings, as well as those from Mišić et al. (2016) deviate from most prior SC-FC studies suggesting that direct SC strength reliably predicts FC strength; and in our case, there are at least two important study differences that may explain some of the disparity. First, in contrast to the majority of previous SC-FC studies that measured streamline connection counts or edge weights (which factor in connection counts, as well as path lengths, and overall white matter volumes), we extracted quantitative SC metrics (i.e., FA, MD, and MWF) from previously-defined white matter ROIs. Although – and perhaps partly due to the fact that – connection counts and edge weighs are highly dependent on node size, seeding bias, and a number of tract-specific anatomical factors (e.g., path length, prevalence of crossing fibers, gyral bias, etc.) [see Sotiropoulos & Zalesky (2017) for a recent review], previous studies have shown that connection count and edge weight tend to be more highly correlated with FC than quantitative measures such as FA (Huang & Ding, 2016). Secondly, and again unlike most prior SC-FC studies, we intentionally constrained our analyses to functionally-connected networks, thereby restricting our SC-FC comparisons to brain regions that are known to have high FC. What is more, we then further constrained our analyses by assessing only those functional nodes for which corresponding white matter atlases were available (i.e., those that have putative structural connections). All else being equal, restricting the dynamic range among our FC and SC values might have been expected to reduce the correspondence between SC and FC compared to whole-brain exploratory studies (Hagmann et al., 2008; Honey et al., 2009; Skudlarski et al., 2008; Stam et al., 2016). For example, whole-brain correlations would be expected to emerge

from the simple fact that many brain regions are known to have no or low SC and FC, while other regions are known to have moderate or high SC and FC. However, the aim of our study was to evaluate whether these SC-FC correlations held up within established networks, and to evaluate the degree of SC-FC coupling within direct and indirect connections within these networks. In this regard, the current study and some of the recent work by Mišić et al. (2016) are the first that we know of to constrain SC-FC relationship analyses to functionally-connected brain regions, specifically large-scale resting state networks; and despite the fact that the functional network connections each had a corresponding structural connection, our analyses revealed a low rate of direct SC-FC coupling, and a surprisingly high rate of indirect SC-FC coupling.

4.2 Rich Club Participation in Structural Connectivity and Functional Connectivity Relationships

The rich club is a set of brain regions comprised of highly centralized, high-degree anatomical hubs that are *rich* in connections to other areas of the brain as well as to one another, thereby forming a *club* (Collin et al., 2014; Senden et al., 2014; van den Heuvel et al., 2012; van den Heuvel & Sporns, 2013a). The SC amongst these regions are thought to link multiple networks – including the default mode and salience networks (van den Heuvel & Sporns, 2013a) – and involve white matter connections that are higher in volume, energy metabolism, and functional connections relative to non-rich club regions (Collin et al., 2014). Careful analysis of our data revealed that a surprisingly high proportion of significant indirect SC-FC relationships involved rich club brain regions, and that the presence of two or more rich club nodes drastically increased the chances that an SC-FC relationship was significant. These results indicate that rich club regions are disproportionately involved in SC-FC coupling within large-scale brain

networks, and further reveal how rich club regions receive, integrate, and circulate information in order to enable large-scale brain function (Collin et al., 2014; Senden et al., 2014; van den Heuvel & Sporns, 2011, 2013a).

The rich club regions that we identified through our SC-FC relationship analysis included the precuneus (where nodes D4, V6, and P3 are located), right superior and middle frontal gyri (R1 and R2, respectively), left and right hippocampi (D8 and D9, respectively), left and right thalamus (P7 and P10, respectively), anterior cingulate cortex (D1), and the right posterior insula (P12), each of which are areas that have been consistently identified as rich club members (Collin et al., 2014; Liao et al., 2013; Senden et al., 2014; van den Heuvel & Sporns, 2013b). The heterogeneity of these regions and their disproportionate participation in SC-FC coupling highlights their capacity for high-volume information processing, an essential role in global brain communication, and the importance of further studying the involvement of these regions in both healthy and diseased brain states.

4.3 SC-FC Coupling Consistency Across SC Metrics

Importantly, the findings that we reported are supported across all three structural metrics: MD, FA, and MWF. For example, the FC strength of connection D4-D5 in the dDMN was significantly correlated with the SC strength from multiple distinct connections within the network as measured using FA, MD, and MWF (Figure 5); moreover, it can be seen in the regression analyses that the combination of all three SC metrics for the same connections account for a significant amount of variance in the FC for D4-D5. Previous SC-FC studies have typically relied exclusively on diffusion-based metrics to infer SC (Bowman et al., 2012; Damoiseaux & Greicius, 2009; Honey et al., 2009; Meier et al., 2016; Mišić et al., 2016). However, our findings illustrate that direct and indirect SC-FC coupling was generally consistent

across multiple SC metrics, both within a single modality (i.e., MD and FA derived from DTI) and across modalities (i.e., MWF derived from MWI). Consistency across SC metrics lends strength to the validity and reliability of the SC-FC relationships identified, and demonstrates the possibility of expanding SC-FC relationship studies beyond diffusion-based approaches to those such as MWI (Alonso-Ortiz et al., 2015; Prasloski et al., 2012).

However, it is worth noting that correlations with MWF produced fewer significant relationships with FC strength relative to the diffusion-based metrics. For instance, in the correlation analyses there were 66 significant SC-FC relationships (direct and indirect) of which 23 were FA-FC, 35 were MD-FC and 8 were MWF-FC. There are three characteristics about MWI that may explain this finding. One is that in relation to DTI, MWI generally has a lower signal-to-noise ratio (Prasloski et al., 2012). Another key factor that differentiates DTI and MWI is that MWI is more specific to myelin, whereas diffusion-based metrics are more general measures of tissue microstructure (Beaulieu & Allen, 1994; MacKay & Laule, 2016). Finally, MWI results may differ from DTI results because MWI is particularly effected by the presence of iron, which can inflate MWF values (Alonso-Ortiz et al., 2015). Such an effect would have been most likely for white matter tracts that meet deep gray matter regions such as the caudate, thalamus and putamen which are commonly richer in iron relative to white matter structures (Pfefferbauma et al., 2012).

4.4 Limitations and Future Directions

As discussed above, our analyses were restricted to network connections that were included in the UManitoba-JHU Functionally-Defined Human White Matter Atlases, which were originally created using white matter tractography methods that are vulnerable to both Type I (false positive) and Type II (false negative) errors (Figley et al., 2015, 2017). Therefore, a given

structural connection may: 1) include some fibers that are part of other connections, and 2) exclude some fibers that are actually part of the given connection (Figley et al., 2015, 2017). Although the analyses in the creation of the atlases did not reveal structural connections between every pair of functionally-connected brain regions, it cannot be assumed that they do not exist.

Another limitation is that the results of this study are based on the simplest measure of resting state FC, where the average bivariate correlation (i.e., between any two functional nodes) was taken throughout the entire 7.5 minute fMRI scan. Over the past few years however, dynamic FC approaches have revealed temporal variations occurring throughout resting state fMRI scans (Calhoun et al., 2014; Hutchison et al., 2013), where FC between network nodes fluctuates between states of stronger and weaker FC (Hindriks et al., 2016; Hutchison et al., 2013). Therefore, future SC-FC studies may wish to investigate, for example, whether relatively static SC measures predict maximum (rather than average) FC strength.

Similarly, in the current study, we took the relatively simple approach of using ROI-based analyses to quantify the average strength of SC (i.e., FA, MD, and MWF) of each connection. However, there may be advantages to using more sophisticated approaches in which quantitative SC metrics are extracted along the length of each tract in order to construct SC profiles (Colby et al., 2012; Walsh et al., 2011; Yeatman et al., 2012). Compared to traditional ROI-based approaches, these along-tract analysis methods should be much more sensitive to small, localized alterations (e.g., SC 'bottlenecks') that could significantly influence FC. Therefore, future SC-FC studies may wish to employ these techniques – perhaps together with dynamic FC methods – in order to examine whether minimum along-tract SC measures predict FC strength.

Taken together, extending SC-FC relationship analyses to along-tract SC and dynamic FC analyses is likely to generate more precise predictions about how SC strength constrains FC

strength within the human brain. It will also be important to consider the involvement of the rich club in these future analyses in order to understand how these anatomical structures might facilitate SC-FC coupling and global brain communication.

5.0 CONCLUSIONS

Elucidating the relationships between brain structure and function is crucial for understanding the large-scale organization underlying the diverse functionality of the human brain. Using a novel application of complementary structural and functional human brain atlases of the same functionally-defined brain networks, we demonstrate that the relationships between SC and FC strength within such networks are not simply one-to-one, but rather emerge in indirect and divergent patterns that are facilitated by rich club regions. Importantly, among functional network nodes with direct structural connections, there was a low rate of correspondence between SC and FC strength; however, a surprisingly high rate of indirect correspondence was observed whereby certain structural connections appeared to support multiple functional connections. Our findings highlight the utility of complementary functionally-defined structural and functional atlases in advancing our knowledge of the structure-function relationships of the human brain. Future research must seek to further establish how dynamic functional configurations arise from relatively static underlying structural configurations in the human connectome, and what implications altered SC-FC relationships might have in terms of diagnosis, treatment and management of brain injury or disease.

6.0 ACKNOWLEDGMENTS

This work was supported by a National Institutes of Health (NIH) R01 Operating Grant, Brain Canada Platform Support Grant, Canadian Natural Sciences and Engineering Research Council (NSERC) Discovery Grant, and NSERC Canada Graduate Scholarship. We would like to thank Teresa Figley from the Department of Radiology at the University of Manitoba for her valuable input on early drafts of the manuscript and for assisting with the figures included in this manuscript. We would also like to thank Loring Chuchmach from the Data Science Platform at the George & Fay Yee Centre for Healthcare Innovation for valuable discussions regarding the statistical analyses utilized in this study.

REFERENCES

Alexander, A. L., Lee, J. E., Lazar, M., & Field, A. S. (2007). Diffusion Tensor Imaging of the Brain. *Neurotherapeutics*, *4*(3), 316–329.

Alonso-Ortiz, E., Levesque, I. R., & Pike, G. B. (2015). MRI-based myelin water imaging: A technical review. *Magnetic Resonance in Medicine*, *73*(1), 70–81. https://doi.org/10.1002/mrm.25198

Ashburner, J., & Friston, K. J. (2005). Unified segmentation. *NeuroImage*, *26*(3), 839–851. https://doi.org/10.1016/j.neuroimage.2005.02.018

Beaulieu, C., & Allen, P. S. (1994). Determinants of anisotropic water diffusion in nerves. *Magnetic Resonance in Medicine*, *31*(4), 394–400. https://doi.org/10.1002/mrm.1910310408

Beg, M. F., Miller, M. I., Trouvé, A., & Younes, L. (2005). Computing Large Deformation Metric Mappings via Geodesic Flows of Diffeomorphisms. *International Journal of Computer Vision*, *61*(2), 139–157. https://doi.org/10.1023/B:VISI.0000043755.93987.aa

Behzadi, Y., Restom, K., Liau, J., & Liu, T. T. (2007). A component based noise correction method (CompCor) for BOLD and perfusion based fMRI. *NeuroImage*, *37*(1), 90–101. https://doi.org/10.1016/j.neuroimage.2007.04.042

Biswal, B., FZ, Y., VM, H., & JS, H. (1995). Functional connectivity in the motor cortex of resting human brain using echo-planar MRI. *Magnetic Resonance in Medicine*, *34*(9), 537–541. https://doi.org/10.1002/mrm.1910340409

Bowman, F. D., Zhang, L., Derado, G., & Chen, S. (2012). Determining functional connectivity using fMRI data with diffusion-based anatomical weighting. *NeuroImage*, *62*(3), 1769–1779. https://doi.org/10.1016/j.neuroimage.2012.05.032

Bressler, S. L., & Menon, V. (2010). Large-scale brain networks in cognition: emerging methods and principles. *Trends in Cognitive Sciences*, *14*(6), 277–290. https://doi.org/10.1016/j.tics.2010.04.004

Buckner, R. L., Andrews-Hanna, J. R., & Schacter, D. L. (2008). The brain's default network: Anatomy, function, and relevance to disease. *Annals of the New York Academy of Sciences*, *1124*, 1–38. https://doi.org/10.1196/annals.1440.011

Calhoun, V. D., Miller, R., Pearlson, G., & Adali, T. (2014). The Chronnectome: Time-Varying Connectivity Networks as the Next Frontier in fMRI Data Discovery. *Neuron*, *84*(2), 262–274. https://doi.org/10.1016/j.neuron.2014.10.015

Choe, A. S., Jones, C. K., Joel, S. E., Muschelli, J., Belegu, V., Caffo, B. S., … Pekar, J. J. (2015). Reproducibility and Temporal Structure in Weekly Resting-State fMRI over a Period of 3.5 Years. *PLOS ONE*, *10*(10), e0140134. https://doi.org/10.1371/journal.pone.0140134

Colby, J. B., Soderberg, L., Lebel, C., Dinov, I. D., Thompson, P. M., & Sowell, E. R. (2012). Along-tract statistics allow for enhanced tractography analysis. *NeuroImage*, *59*(4), 3227–3242. https://doi.org/10.1016/j.neuroimage.2011.11.004

Collin, G., Sporns, O., Mandl, R. C. W., & van den Heuvel, M. P. (2014). Structural and functional aspects relating to cost and benefit of rich club organization in the human cerebral cortex. *Cerebral Cortex (New York, N.Y. : 1991)*, *24*(9), 2258–67. https://doi.org/10.1093/cercor/bht064

Damoiseaux, J., & Greicius, M. (2009). Greater than the sum of its parts: a review of studies combining structural connectivity and resting-state functional connectivity. *Brain Structure and Function*, *213*(6), 525–533. https://doi.org/10.1007/s00429-009-0208-6

Deco, G., Jirsa, V. K., & McIntosh, A. R. (2011). Emerging concepts for the dynamical organization of resting-state activity in the brain. *Nature Reviews. Neuroscience*, *12*(1), 43–56. https://doi.org/10.1038/nrn2961

Deco, G., Ponce-Alvarez, a., Mantini, D., Romani, G. L., Hagmann, P., & Corbetta, M. (2013). Resting-State Functional Connectivity Emerges from Structurally and Dynamically Shaped Slow Linear Fluctuations. *Journal of Neuroscience*, *33*(27), 11239–11252. https://doi.org/10.1523/JNEUROSCI.1091-13.2013

Deco, G., Senden, M., & Jirsa, V. (2012). How anatomy shapes dynamics: a semi-analytical study of the brain at rest by a simple spin model. *Frontiers in Computational Neuroscience*, *6*(September), 1–7. https://doi.org/10.3389/fncom.2012.00068

Farrell, J. A. D., Landman, B. A., Jones, C. K., Smith, S. A., Prince, J. L., van Zijl, P. C. M., & Mori, S. (2007). Effects of signal-to-noise ratio on the accuracy and reproducibility of diffusion tensor imaging–derived fractional anisotropy, mean diffusivity, and principal eigenvector measurements at 1.5T. *Journal of Magnetic Resonance Imaging*, *26*(3), 756–767. https://doi.org/10.1002/jmri.21053

Figley, C. R., Asem, J. S. A., Levenbaum, E. L., & Courtney, S. M. (2016). Effects of Body Mass Index and Body Fat Percent on Default Mode, Executive Control, and Salience Network Structure and Function. *Frontiers in Neuroscience*, *10*, 234. https://doi.org/10.3389/fnins.2016.00234

Figley, T. D., Bhullar, N., Courtney, S. M., & Figley, C. R. (2015). Probabilistic atlases of default mode, executive control and salience network white matter tracts: an fMRI-guided diffusion tensor imaging and tractography study. *Frontiers in Human Neuroscience*, *9*(November), Article 585. https://doi.org/10.3389/fnhum.2015.00585

Figley, T. D., Mortazavi Moghadam, B., Bhullar, N., Kornelsen, J., Courtney, S., & Figley, C. R. (2017). Probabilistic white matter atlases of human auditory, basal ganglia, language, precuneus, sensorimotor, visual, and visuospatial networks. *Frontiers in Human Neuroscience*, *11*, 306. https://doi.org/10.3389/FNHUM.2017.00306

Greicius, M. D., Supekar, K., Menon, V., & Dougherty, R. F. (2009). Resting-state functional connectivity reflects structural connectivity in the default mode network. *Cerebral Cortex*, *19*(1), 72–78. https://doi.org/10.1093/cercor/bhn059

Hagmann, P., Cammoun, L., Gigandet, X., Meuli, R., Honey, C., Wedeen, V., & Sporns, O. (2008). Mapping the Structural Core of Human Cerebral Cortex. *PLoS Biology*, *6*(7), e159. https://doi.org/10.1371/journal.pbio.0060159

Hennig, J., Weigel, M., & Scheffler, K. (2003). Multiecho sequences with variable refocusing flip angles: Optimization of signal behavior using smooth transitions between pseudo steady states (TRAPS). *Magnetic Resonance in Medicine*, *49*(3), 527–535. https://doi.org/10.1002/mrm.10391

Hermundstad, A. M., Bassett, D. S., Brown, K. S., Aminoff, E. M., Clewett, D., Freeman, S., … Carlson, J. M. (2013). Structural foundations of resting-state and task-based functional connectivity in the human brain. *Proceedings of the National Academy of Sciences of the United States of America*, *110*(15), 6169–74. https://doi.org/10.1073/pnas.1219562110

Hermundstad, A. M., Brown, K. S., Bassett, D. S., Aminoff, E. M., Frithsen, A., Johnson, A., … Carlson, J. M. (2014). Structurally-Constrained Relationships between Cognitive States in the Human Brain. *PLoS Computational Biology*, *10*(5), e1003591. https://doi.org/10.1371/journal.pcbi.1003591

Hindriks, R., Adhikari, M. H., Murayama, Y., Ganzetti, M., Mantini, D., Logothetis, N. K., &

Deco, G. (2016). Can sliding-window correlations reveal dynamic functional connectivity in resting-state fMRI? *NeuroImage*, *127*, 242–256. https://doi.org/10.1016/j.neuroimage.2015.11.055

Honey, C., Kötter, R., Breakspear, M., & Sporns, O. (2007). Network structure of cerebral cortex shapes functional connectivity on multiple time scales. *Proceedings of the National Academy of Sciences of the United States of America*, *104*(24), 10240–5. https://doi.org/10.1073/pnas.0701519104

Honey, C., Sporns, O., Cammoun, L., Gigandet, X., Thiran, J., Meuli, R., & Hagmann, P. (2009). Predicting human resting-state functional connectivity from structural connectivity. *Proceedings of the National Academy of Sciences*, *106*(6), 2035–2040.

Honey, C., Thivierge, J.-P., & Sporns, O. (2010). Can structure predict function in the human brain? *NeuroImage*, *52*(3), 766–776. https://doi.org/10.1016/j.neuroimage.2010.01.071

Huang, H., & Ding, M. (2016). Linking functional connectivity and structural connectivity quantitatively: A comparison of methods. *Brain Connectivity*, *6*(2), 1–10. https://doi.org/10.1089/brain.2015.0382

Hutchison, R. M., Womelsdorf, T., Allen, E. A., Bandettini, P. A., Calhoun, V. D., Corbetta, M., … Chang, C. (2013). Dynamic functional connectivity: Promise, issues, and interpretations. *NeuroImage*, *80*, 360–378. https://doi.org/10.1016/j.neuroimage.2013.05.079

Hutchison, R. M., Womelsdorf, T., Gati, J. S., Everling, S., & Menon, R. S. (2013). Resting-state networks show dynamic functional connectivity in awake humans and anesthetized macaques. *Human Brain Mapping*, *34*(9), 2154–2177. https://doi.org/10.1002/hbm.22058

Khalsa, S., Mayhew, S. D., Chechlacz, M., Bagary, M., & Bagshaw, A. P. (2014). The structural and functional connectivity of the posterior cingulate cortex: Comparison between deterministic and probabilistic tractography for the investigation of structure–function relationships. *NeuroImage*, *102*, 118–127. https://doi.org/10.1016/j.neuroimage.2013.12.022

Koch, M. A., Norris, D. G., & Hund-Georgiadis, M. (2002). An Investigation of Functional and Anatomical Connectivity Using Magnetic Resonance Imaging. *NeuroImage*, *16*(1), 241–250. https://doi.org/10.1006/nimg.2001.1052

Liao, X.-H., Xia, M.-R., Xu, T., Dai, Z.-J., Cao, X.-Y., Niu, H.-J., … He, Y. (2013). Functional brain hubs and their test–retest reliability: A multiband resting-state functional MRI study. *NeuroImage*, *83*, 969–982. https://doi.org/10.1016/j.neuroimage.2013.07.058

MacKay, A. L., & Laule, C. (2016). Magnetic Resonance of Myelin Water: An in vivo Marker for Myelin. *Brain Plasticity*, *2*(1), 71–91. https://doi.org/10.3233/BPL-160033

Mazziotta, J. C., Toga, A. W., Evans, A., Fox, P., & Lancaster, J. (1995). A Probabilistic Atlas of the Human Brain: Theory and Rationale for Its Development: The International Consortium for Brain Mapping (ICBM). *NeuroImage*, *2*(2), 89–101. https://doi.org/10.1006/nimg.1995.1012

Meier, J., Tewarie, P., Hillebrand, A., Douw, L., van Dijk, B. W., Stufflebeam, S. M., & Van Mieghem, P. (2016). A Mapping Between Structural and Functional Brain Networks. *Brain Connectivity*, *31*(0), brain.2015.0408. https://doi.org/10.1089/brain.2015.0408

Mišić, B., Betzel, R. F., de Reus, M. A., van den Heuvel, M. P., Berman, M. G., McIntosh, A. R., & Sporns, O. (2016). Network-Level Structure-Function Relationships in Human Neocortex. *Cerebral Cortex*, (April), bhw089. https://doi.org/10.1093/cercor/bhw089

Park, H.-J., & Friston, K. (2013). Structural and Functional Brain Networks: From Connections to Cognition. *Science*, *342*(6158), 1238411–1238411.

https://doi.org/10.1126/science.1238411
Pfefferbauma, A., Adalsteinssonc, E., Rohlfinga, T., & Sullivan, E. (2012). Diffusion tensor imaging of deep gray matter brain structures: Effects of age and iron concentration. *Neurobiol Aging*, *31*(3), 1–19. https://doi.org/10.1038/cdd.2010.172.MicroRNAs
Prasloski, T., Rauscher, A., MacKay, A. L., Hodgson, M., Vavasour, I. M., Laule, C., & Mädler, B. (2012). Rapid whole cerebrum myelin water imaging using a 3D GRASE sequence. *NeuroImage*, *63*(1), 533–539. https://doi.org/10.1016/j.neuroimage.2012.06.064
Rubinov, M., & Sporns, O. (2010). Complex network measures of brain connectivity: Uses and interpretations. *NeuroImage*, *52*(3), 1059–1069. https://doi.org/10.1016/j.neuroimage.2009.10.003
Seeley, W. W., Menon, V., Schatzberg, A. F., Keller, J., Glover, G. H., Kenna, H., … Greicius, M. D. (2007). Dissociable intrinsic connectivity networks for salience processing and executive control. *J Neurosci*, *27*(9), 2349–2356. https://doi.org/10.1523/JNEUROSCI.5587-06.2007
Senden, M., Deco, G., de Reus, M. A., Goebel, R., & van den Heuvel, M. P. (2014). Rich club organization supports a diverse set of functional network configurations. *NeuroImage*, *96*, 174–182. https://doi.org/10.1016/j.neuroimage.2014.03.066
Shirer, W. R., Ryali, S., Rykhlevskaia, E., Menon, V., & Greicius, M. D. (2012). Decoding subject-driven cognitive states with whole-brain connectivity patterns. *Cerebral Cortex (New York, N.Y. : 1991)*, *3211*(January).
Skudlarski, P., Jagannathan, K., Calhoun, V. D., Hampson, M., Skudlarska, B. A., & Pearlson, G. (2008). Measuring brain connectivity: Diffusion tensor imaging validates resting state temporal correlations. *NeuroImage*, *43*(3), 554–561. https://doi.org/10.1016/j.neuroimage.2008.07.063
Smith, S. M., Vidaurre, D., Beckmann, C. F., Glasser, M. F., Jenkinson, M., Miller, K. L., … Van Essen, D. C. (2013). Functional connectomics from resting-state fMRI. *Trends in Cognitive Sciences*, *17*(12), 666–682. https://doi.org/10.1016/j.tics.2013.09.016
Sotiropoulos, S. N., & Zalesky, A. (2017). Building connectomes using diffusion MRI: why, how and but. *NMR in Biomedicine*, e3752. https://doi.org/10.1002/nbm.3752
Stam, C. J., van Straaten, E. C. W., Van Dellen, E., Tewarie, P., Gong, G., Hillebrand, A., … Van Mieghem, P. (2016). The relation between structural and functional connectivity patterns in complex brain networks. *International Journal of Psychophysiology*, *103*, 149–160. https://doi.org/10.1016/j.ijpsycho.2015.02.011
van den Heuvel, M. P., Kahn, R. S., Goni, J., & Sporns, O. (2012). High-cost, high-capacity backbone for global brain communication. *Proceedings of the National Academy of Sciences*, *109*(28), 11372–11377. https://doi.org/10.1073/pnas.1203593109
van den Heuvel, M. P., Mandl, R. C. W., Kahn, R. S., & Hulshoff Pol, H. E. (2009). Functionally linked resting-state networks reflect the underlying structural connectivity architecture of the human brain. *Human Brain Mapping*, *30*(10), 3127–3141. https://doi.org/10.1002/hbm.20737
van den Heuvel, M. P., Mandl, R., Luigjes, J., & Hulshoff Pol, H. (2008). Microstructural Organization of the Cingulum Tract and the Level of Default Mode Functional Connectivity. *Journal of Neuroscience*, *28*(43), 10844–10851. https://doi.org/10.1523/JNEUROSCI.2964-08.2008
van den Heuvel, M. P., & Sporns, O. (2011). Rich-Club Organization of the Human Connectome. *Journal of Neuroscience*, *31*(44), 15775–15786.

https://doi.org/10.1523/JNEUROSCI.3539-11.2011
van den Heuvel, M. P., & Sporns, O. (2013a). An Anatomical Substrate for Integration among Functional Networks in Human Cortex. *Journal of Neuroscience*, *33*(36), 14489–14500. https://doi.org/10.1523/JNEUROSCI.2128-13.2013
van den Heuvel, M. P., & Sporns, O. (2013b). Network hubs in the human brain. *Trends in Cognitive Sciences*, *17*(12), 683–96. https://doi.org/10.1016/j.tics.2013.09.012
Walsh, M., Montojo, C. A., Sheu, Y.-S., Marchette, S. A., Harrison, D. M., Newsome, S. D., … Courtney, S. M. (2011). Object Working Memory Performance Depends on Microstructure of the Frontal-Occipital Fasciculus. *Brain Connectivity*, *1*(4), 317–329. https://doi.org/10.1089/brain.2011.0037
Yeatman, J. D., Dougherty, R. F., Myall, N. J., Wandell, B. A., Feldman, H. M., Basser, P., … Holmes, A. (2012). Tract Profiles of White Matter Properties: Automating Fiber-Tract Quantification. *PLoS ONE*, *7*(11), e49790. https://doi.org/10.1371/journal.pone.0049790

Chapter 4: Brief Discussion

The purpose of this thesis was to expand our understanding of how structural connectivity (SC) couples with functional connectivity (FC) within the functional hierarchy of the human brain, specifically in large-scale resting state networks. In order to do so, I applied a complementary pair of functionally-defined structural (UManitoba-JHU Functionally-Defined Human White Matter Atlas; Figley et al., 2015) and functional (Stanford functional-MRI Atlas; Shirer et al., 2012) atlases of six well-established resting state brain networks to two types of SC data (diffusion tensor imaging [DTI] and myelin water imaging [MWI]) and one type of FC data (resting state functional-MRI [rs-fMRI]), respectively. These networks included the dorsal and ventral default mode network (dDMN, vDMN), left and right executive control network (lECN, rECN), and anterior and posterior salience network (aSN, pSN). I found that within each network, direct relationships between SC and FC strength were weak overall, but there were strong indirect associations between SC and FC wherein the SC from a given connection correlated with the FC of partially-overlapping (sharing 1/2 nodes) or non-overlapping (sharing 0/2 nodes) connections within the same network. Moreover, my results also revealed that for each SC-FC combination, the likelihood of identifying a significant association drastically increased with the presence of two or more rich club nodes (four possible nodes for each SC-FC combination).

Although my findings contradict the notion that strong direct SC between two given brain regions should correlate with FC between those same regions (Damoiseaux & Greicius, 2009; Honey et al., 2010), they are corroborated by a similar recent SC-FC coupling study (Mišić et al., 2016) that also found that SC indirectly supports FC within resting state networks. Moreover, although many previous studies suggest direct SC-FC correspondence at connections where SC

and FC are both present (Greicius et al., 2009; Hagmann et al., 2008; Honey et al., 2009; Huang & Ding, 2016; Khalsa et al., 2014; Koch et al., , 2002), these prior studies also suggested that indirect SC-FC coupling must account for some degree of FC at the network level due to the presence of functional connections without direct structural connections. It is through our novel approach, which only looked at network connections with direct SC and FC (restricting variance in the FC degree), that we identified indirect correspondence at the network connection level, wherein the FC strength from a given connection was associated with the SC strength from partially-overlapping and/or non-overlapping connections within the same network. Importantly, even though the functional network connections that I examined each had a corresponding structural connection, there was a low rate of direct correspondence between the SC and FC metrics for each connection but a high rate of indirect correspondence. What I present in this thesis is a systematic investigation of the SC-FC coupling patterns within individual network connections, which lends novel empirical evidence to the notion that large-scale SC can provide indirect and divergent support to FC within the human brain.

Furthermore, I found that when at least two network nodes were located in a rich club region in an SC-FC comparison (four nodes total, two from the SC connection and two from the FC connection), there was a much greater probability that the relationship was significant. The well-established rich club brain regions that were involved in the majority of the strong SC-FC relationships included the precuneus, right superior and middle frontal gyri, left and right thalamus, anterior cingulate cortex, and the right posterior insula (van den Heuvel et al., 2012; van den Heuvel & Sporns, 2011). Not only are these regions regarded as structural and functional brain hubs (Hagmann et al., 2008; van den Heuvel et al., 2012; van den Heuvel & Sporns, 2011), but they are also functionally-diverse associative regions (Cavanna & Trimble,

2006; Glimcher & Lau, 2005; Knierim, 2015; Lavin et al., 2013; Nieuwenhuys, 2012; Stevens, Hurley, & Taber, 2011; Tamminga, 2004) that consume glucose at significantly higher metabolic rates relative to non-rich club regions (Collin et al., 2014). For instance, physiological and psychological studies have identified the precuneus as a major association area that integrates various external stimuli from the environment with internal information in order to aid tasks such as visuo-spatial imagery (Suzuki et al.,, 1998), episodic memory retrieval (Shallice et al., 1994), and self-processing operations (Cavanna & Trimble, 2006; Kjaer et al., 2002). These findings align with the neuroimaging findings that show: 1) there are DMN and SN nodes located in the precuneus (Shirer et al., 2012), and 2) these networks are involved in functions such as taking the perspective of others (Buckner et al., 2008) and deciding our next action based on elaborate sensory information (Seeley et al., 2007). Another example, the frontal lobes, specifically the superior and middle frontal gyri have been implicated in a number of cognitive and executive functioning processes, such as attention and making behavioural decisions based on external and internal stimuli (Tamminga, 2004); and these physiological and behavioural studies converge with fMRI studies that have identified nodes of the ECN within the frontal lobe (Shirer et al., 2012).

It seems to follow that such a task, mediating SC-FC coupling for global brain communication, would require high amounts of energy and white matter pathways – in fact, together these rich club regions are regarded as a "high cost, high capacity backbone" that supports global brain communication (van den Heuvel et al., 2012). These findings also converge with clinical studies that found SC-FC decoupling in pediatric onset multiple sclerosis (Akbar et al., 2016), relapsing remitting multiple sclerosis (Zhou et al., 2014) and major depressive disorder (Kwaasteniet et al., 2012) was most significant in connections involving the precuneus

and anterior cingulate cortex. Overall, this thesis helps set an empirical foundation for the notion that SC indirectly supports global FC in the human brain through a select set rich club brain regions and connections that are associated with various cognitive, sensory, and behavioural processes.

Chapter 5: Future Directions

The results of this study are based on simple static definitions of functional connectivity (FC) that work under the assumption that FC is constant throughout the entire 7.5 minute fMRI scan. Over the past few years, a novel approach has revealed dynamic features of FC over the duration of the scan (Calhoun et al., 2014; Hutchison et al., 2013), wherein the FC of network nodes has been found to vary temporally between states of stronger and weaker FC (Hindriks et al., 2016; Hutchison et al., 2013). Moreover, pathological studies have found that dynamic FC reveals abnormalities in FC that would be missed using a classic static FC approach (Demirtaş et al., 2016). Given these macroscopic temporal changes in FC over time scales of several minutes, and that macroscopic structural connectivity (SC) is relatively stable, the question arises: How does dynamic functional connectivity emerge from relatively static underlying SC?

Another limitation of the current study is the use of a region-of-interest (ROI-based) analysis to quantify SC. A small number of studies have revealed advantages to along-tract analyses in which quantitative SC metrics are extracted along the length of SC tracts to construct characteristic profiles (Colby et al., 2012; Walsh et al., 2011; Yeatman et al., 2012). In comparison to traditional ROI-based procedures, the tract-based approach allows for a more accurate measure of SC within large white matter regions with preserved sensitivity to small localized alterations that ROI-analyses could miss. When examining a white matter pathway between two brain regions, ROI-based procedures simply produce a single mean SC metric (e.g., mean FA or MD) representative of the SC within the entire tract, whereas the tract-based analysis will produce a curve of the SC metric composed of a distribution of multiple values representing SC from the weakest to the strongest point along the tract of the white matter pathway. It is important for future studies to investigate the relationship between SC and FC

(static and dynamic) within the human brain using along-tract analyses in order to examine how FC relates to minimum and maximum SC. By extending SC-FC relationship analyses to tract-based and dynamic connectivity measures (respectively), we can make more precise predictions about how SC constrains FC within the human brain.

Chapter 6: Conclusions

Magnetic resonance imaging (MRI) is a powerful technique that can be used to better understand how the macroscale structure of the human brain supports such a great variety of functions. Structural MRI methods including diffusion tensor imaging (DTI) and myelin water imaging (MWI) can be used to quantify the strength of structural connections throughout the brain. Concurrently, resting state functional MRI (rs-fMRI) can be used to quantify the strength of functional connections throughout the brain. Although prior studies have examined relationships between structural connectivity (SC) and functional connectivity (FC) amongst anatomically-defined brain regions, they have not systematically addressed SC-FC relationships with consideration of human brain organization in the form of distributed functional resting state or large-scale networks. We introduced a novel application of complementary functionally-defined structural and functional brain atlases, applied respective region-of-interest analyses to DTI, MWI, and rs-fMRI data, and examined SC-FC relationships using linear correlation and regression analyses. This thesis provides convergent evidence across multiple SC metrics for indirect and divergent SC-FC coupling within six well-established large-scale networks: the dorsal and ventral default mode networks, left and right executive control networks, and the anterior and posterior salience networks. The work detailed in this thesis adds to our understanding of how structure supports function within the human brain.

References

Abbott, A. E., Nair, A., Keown, C. L., Datko, M., Jahedi, A., Fishman, I., & Müller, R. A. (2016). Patterns of Atypical Functional Connectivity and Behavioral Links in Autism Differ between Default, Salience, and Executive Networks. *Cerebral Cortex*, *26*(10), 4034–4045. https://doi.org/10.1093/cercor/bhv191

Akbar, N., Giorgio, A., Till, C., Sled, J. G., Doesburg, S. M., Stefano, N. De, & Banwell, B. (2016). Alterations in Functional and Structural Connectivity in Pediatric-Onset Multiple Sclerosis, 1–14. https://doi.org/10.1371/journal.pone.0145906

Alexander, A. L., Lee, J. E., Lazar, M., & Field, A. S. (2007). Diffusion Tensor Imaging of the Brain. *Neurotherapeutics*, *4*(3), 316–329.

Alonso-Ortiz, E., Levesque, I. R., & Pike, G. B. (2015). MRI-based myelin water imaging: A technical review. *Magnetic Resonance in Medicine*, *73*(1), 70–81. https://doi.org/10.1002/mrm.25198

Amunts, K., & Zilles, K. (2012). Architecture and organizational principles of Broca's region. *Trends in Cognitive Sciences*, *16*(8), 418–426. https://doi.org/10.1016/j.tics.2012.06.005

Ashburner, J., & Friston, K. J. (2005). Unified segmentation. *NeuroImage*, *26*(3), 839–851. https://doi.org/10.1016/j.neuroimage.2005.02.018

Barbas, H. (2015). General Cortical and Special Prefrontal Connections: Principles from Structure to Function. *Annual Review of Neuroscience*, *38*(1), 269–289. https://doi.org/10.1146/annurev-neuro-071714-033936

Basser, P. J., Mattiello, J., & LeBihan, D. (1994). MR diffusion tensor spectroscopy and imaging. *Biophysical Journal*, *66*(1), 259–67. https://doi.org/10.1016/S0006-3495(94)80775-1

Bassett, D. S., & Bullmore, E. D. (2006). Small-World Brain Networks, *12*(6). https://doi.org/10.1177/1073858406293182

Beaulieu, C. (2002). The basis of anisotropic water diffusion in the nervous system - A technical review. *NMR in Biomedicine*, *15*(7–8), 435–455. https://doi.org/10.1002/nbm.782

Beaulieu, C., & Allen, P. S. (1994). Determinants of anisotropic water diffusion in nerves. *Magnetic Resonance in Medicine*, *31*(4), 394–400. https://doi.org/10.1002/mrm.1910310408

Beg, M. F., Miller, M. I., Trouvé, A., & Younes, L. (2005). Computing Large Deformation Metric Mappings via Geodesic Flows of Diffeomorphisms. *International Journal of Computer Vision*, *61*(2), 139–157. https://doi.org/10.1023/B:VISI.0000043755.93987.aa

Behzadi, Y., Restom, K., Liau, J., & Liu, T. T. (2007). A component based noise correction method (CompCor) for BOLD and perfusion based fMRI. *NeuroImage*, *37*(1), 90–101. https://doi.org/10.1016/j.neuroimage.2007.04.042

Biswal, B., FZ, Y., VM, H., & JS, H. (1995). Functional connectivity in the motor cortex of resting human brain using echo-planar MRI. *Magnetic Resonance in Medicine*, *34*(9), 537–541. https://doi.org/10.1002/mrm.1910340409

Bowman, F. D., Zhang, L., Derado, G., & Chen, S. (2012). Determining functional connectivity using fMRI data with diffusion-based anatomical weighting. *NeuroImage*, *62*(3), 1769–

1779. https://doi.org/10.1016/j.neuroimage.2012.05.032

Bressler, S. L., & Menon, V. (2010). Large-scale brain networks in cognition: emerging methods and principles. *Trends in Cognitive Sciences*, *14*(6), 277–290. https://doi.org/10.1016/j.tics.2010.04.004

Broadmann, K. (1909). Vergleichende Lokalisationslehre der Grosshirnrinde. *Leipzig: Johann Ambrosius Barth*.

Buckner, R. L., Andrews-Hanna, J. R., & Schacter, D. L. (2008). The brain's default network: Anatomy, function, and relevance to disease. *Annals of the New York Academy of Sciences*, *1124*, 1–38. https://doi.org/10.1196/annals.1440.011

Buckner, R. L., Krienen, F. M., & Yeo, B. T. T. (2013). Opportunities and limitations of intrinsic functional connectivity MRI. *Nature Neuroscience*, *16*(7), 832–837. https://doi.org/10.1038/nn.3423

Bullmore, E., & Sporns, O. (2009). Complex brain networks : graph theoretical analysis of structural and functional systems, *10*(maRcH). https://doi.org/10.1038/nrn2575

Caballero, B. (2013). *Encyclopedia of human nutrition* (3rd ed.). Amsterdam: Elsevier.

Calhoun, V. D., Miller, R., Pearlson, G., & Adali, T. (2014). The Chronnectome: Time-Varying Connectivity Networks as the Next Frontier in fMRI Data Discovery. *Neuron*, *84*(2), 262–274. https://doi.org/10.1016/j.neuron.2014.10.015

Campbell, A. (1903). Histological Studies on Cerebral Localisation. *Proceedings of the Royal Society of London*, *72*(477–486), 488–492. https://doi.org/10.1098/rspl.1903.0077

Cavanna, A. E., & Trimble, M. R. (2006). The precuneus: A review of its functional anatomy and behavioural correlates. *Brain*, *129*(3), 564–583. https://doi.org/10.1093/brain/awl004

Chiang, S., Stern, J. M., Engel, J., & Haneef, Z. (2015). Structural – functional coupling changes in temporal lobe epilepsy. *Brain Research*, *1616*, 45–57. https://doi.org/10.1016/j.brainres.2015.04.052

Choe, A. S., Jones, C. K., Joel, S. E., Muschelli, J., Belegu, V., Caffo, B. S., … Milham, M. (2015). Reproducibility and Temporal Structure in Weekly Resting-State fMRI over a Period of 3.5 Years. *PLOS ONE*, *10*(10), e0140134. https://doi.org/10.1371/journal.pone.0140134

Christian, P., Edward, F., & Orleans, N. (1988). Electrophysiological Evidence From Glutamate Microapplications for Local Excitatory Circuits in the CA1 Area of Rat Hippocampal Slices, *59*(I).

Colby, J. B., Soderberg, L., Lebel, C., Dinov, I. D., Thompson, P. M., & Sowell, E. R. (2012). Along-tract statistics allow for enhanced tractography analysis. *NeuroImage*, *59*(4), 3227–3242. https://doi.org/10.1016/j.neuroimage.2011.11.004

Cole, D. M., Smith, S. M., & Beckmann, C. M. (2010). Advances and pitfalls in the analysis and interpretation of resting-state FMRI data. *Frontiers in Systems Neuroscience*, *4*(April), 1–15. https://doi.org/10.3389/fnsys.2010.00008

Collin, G., Sporns, O., Mandl, R. C. W., & van den Heuvel, M. P. (2014). Structural and functional aspects relating to cost and benefit of rich club organization in the human cerebral cortex. *Cerebral Cortex (New York, N.Y. : 1991)*, *24*(9), 2258–67.

https://doi.org/10.1093/cercor/bht064

Concha, L., Livy, D. J., Beaulieu, C., Wheatley, B. M., & Gross, D. W. (2010). In Vivo Diffusion Tensor Imaging and Histopathology of the Fimbria-Fornix in Temporal Lobe Epilepsy. *The Journal of Neuroscience*, *30*(3), 996–1002. https://doi.org/10.1523/JNEUROSCI.1619-09.2010

Craddock, R. C., Jbabdi, S., Yan, C., Vogelstein, J., & Milham, M. P. (2014). Imaging human connectomes at the macroscale. *NIH Public Access*, *10*(6), 524–539. https://doi.org/10.1038/nmeth.2482.Imaging

Damoiseaux, J., & Greicius, M. (2009). Greater than the sum of its parts: a review of studies combining structural connectivity and resting-state functional connectivity. *Brain Structure and Function*, *213*(6), 525–533. https://doi.org/10.1007/s00429-009-0208-6

De Luca, M., Beckmann, C. F., De Stefano, N., Matthews, P. M., & Smith, S. M. (2006). fMRI resting state networks define distinct modes of long-distance interactions in the human brain. *NeuroImage*, *29*(4), 1359–1367. https://doi.org/10.1016/j.neuroimage.2005.08.035

Deco, G., Jirsa, V. K., & McIntosh, A. R. (2011). Emerging concepts for the dynamical organization of resting-state activity in the brain. *Nature Reviews. Neuroscience*, *12*(1), 43–56. https://doi.org/10.1038/nrn2961

Deco, G., Ponce-Alvarez, a., Mantini, D., Romani, G. L., Hagmann, P., & Corbetta, M. (2013). Resting-State Functional Connectivity Emerges from Structurally and Dynamically Shaped Slow Linear Fluctuations. *Journal of Neuroscience*, *33*(27), 11239–11252. https://doi.org/10.1523/JNEUROSCI.1091-13.2013

Deco, G., Senden, M., & Jirsa, V. (2012). How anatomy shapes dynamics: a semi-analytical study of the brain at rest by a simple spin model. *Frontiers in Computational Neuroscience*, *6*(September), 1–7. https://doi.org/10.3389/fncom.2012.00068

Demirtaş, M., Tornador, C., Falcón, C., López-Solà, M., Hernández-Ribas, R., Pujol, J., … Deco, G. (2016). Dynamic functional connectivity reveals altered variability in functional connectivity among patients with major depressive disorder. *Human Brain Mapping*, *37*(8), 2918–2930. https://doi.org/10.1002/hbm.23215

Elston, G. N. (2003). Cortex, Cognition and the Cell: New Insights into the Pyramidal Neuron and Prefrontal Function. *Cerebral Cortex*, *13*(11), 1124–1138. https://doi.org/10.1093/cercor/bhg093

Farrell, J. A. D., Landman, B. A., Jones, C. K., Smith, S. A., Prince, J. L., van Zijl, P. C. M., & Mori, S. (2007). Effects of signal-to-noise ratio on the accuracy and reproducibility of diffusion tensor imaging–derived fractional anisotropy, mean diffusivity, and principal eigenvector measurements at 1.5T. *Journal of Magnetic Resonance Imaging*, *26*(3), 756–767. https://doi.org/10.1002/jmri.21053

Feldman, H., Yeatman, J., Lee, E., Barde, L., & Gaman-Bean, S. (2014). Diffusion Tensor Imaging: A review for Pediatric Researchers and Clinicians. *J Dev Behav Pediatr*, *31*(4), 346–356. https://doi.org/10.1097/DBP.0b013e3181dcaa8b.Diffusion

Ferguson, S. M., & Neumaier, J. F. (2015). Using DREADDs to investigate addiction behaviors. *Current Opinion in Behavioral Sciences*, *2*, 69–72. https://doi.org/10.1016/j.cobeha.2014.09.004

Figley, C. R., Asem, J. S. A., Levenbaum, E. L., & Courtney, S. M. (2016). Effects of Body Mass Index and Body Fat Percent on Default Mode, Executive Control, and Salience Network Structure and Function. *Frontiers in Neuroscience*, *10*, 234. https://doi.org/10.3389/fnins.2016.00234

Figley, T. D., Bhullar, N., Courtney, S. M., & Figley, C. R. (2015). Probabilistic atlases of default mode, executive control and salience network white matter tracts: an fMRI-guided diffusion tensor imaging and tractography study. *Frontiers in Human Neuroscience*, *9*(November), Article 585. https://doi.org/10.3389/fnhum.2015.00585

Figley, T. D., Mortazavi Moghadam, B., Bhullar, N., Kornelsen, J., Courtney, S., & Figley, C. R. (2017). Probabilistic white matter atlases of human auditory, basal ganglia, language, precuneus, sensorimotor, visual, and visuospatial networks. *Frontiers in Human Neuroscience*, *11*, 306. https://doi.org/10.3389/FNHUM.2017.00306

Fox, P. T., & Raichle, M. E. (1986). Focal physiological uncoupling of cerebral blood flow and oxidative metabolism during somatosensory stimulation in human subjects. *Proceedings of the National Academy of Sciences of the United States of America*, *83*(February 1986), 1140–4. https://doi.org/10.1073/pnas.83.4.1140

Glimcher, P. W., & Lau, B. (2005). Rethinking the thalamus. *Nature Neuroscience*, *8*(8), 983–984. https://doi.org/10.1038/nn0805-983

Greicius, M. D., Supekar, K., Menon, V., & Dougherty, R. F. (2009). Resting-state functional connectivity reflects structural connectivity in the default mode network. *Cerebral Cortex*, *19*(1), 72–78. https://doi.org/10.1093/cercor/bhn059

Hagmann, P., Cammoun, L., Gigandet, X., Meuli, R., Honey, C., Wedeen, V., & Sporns, O. (2008). Mapping the Structural Core of Human Cerebral Cortex. *PLoS Biology*, *6*(7), e159. https://doi.org/10.1371/journal.pbio.0060159

Harriger, L., van den Heuvel, M. P., Sporns, O., Sporns, O., Chialvo, D., Kaiser, M., … Kötter, R. (2012). Rich Club Organization of Macaque Cerebral Cortex and Its Role in Network Communication. *PLoS ONE*, *7*(9), e46497. https://doi.org/10.1371/journal.pone.0046497

Hawellek, D. J., Hipp, J. F., Lewis, C. M., Corbetta, M., & Engel, A. K. (2011). Increased functional connectivity indicates the severity of cognitive impairment in multiple sclerosis. *Proceedings of the National Academy of Sciences*, *108*(47), 1–7. https://doi.org/10.1073/pnas.1110024108/-/DCSupplemental.www.pnas.org/cgi/doi/10.1073/pnas.1110024108

Hennig, J., Weigel, M., & Scheffler, K. (2003). Multiecho sequences with variable refocusing flip angles: Optimization of signal behavior using smooth transitions between pseudo steady states (TRAPS). *Magnetic Resonance in Medicine*, *49*(3), 527–535. https://doi.org/10.1002/mrm.10391

Hermundstad, A. M., Bassett, D. S., Brown, K. S., Aminoff, E. M., Clewett, D., Freeman, S., … Carlson, J. M. (2013). Structural foundations of resting-state and task-based functional connectivity in the human brain. *Proceedings of the National Academy of Sciences of the United States of America*, *110*(15), 6169–74. https://doi.org/10.1073/pnas.1219562110

Hermundstad, A. M., Brown, K. S., Bassett, D. S., Aminoff, E. M., Frithsen, A., Johnson, A., … Carlson, J. M. (2014). Structurally-Constrained Relationships between Cognitive States in

the Human Brain. *PLoS Computational Biology*, *10*(5), e1003591. https://doi.org/10.1371/journal.pcbi.1003591

Hindriks, R., Adhikari, M. H., Murayama, Y., Ganzetti, M., Mantini, D., Logothetis, N. K., & Deco, G. (2016). Can sliding-window correlations reveal dynamic functional connectivity in resting-state fMRI? *NeuroImage*, *127*, 242–256. https://doi.org/10.1016/j.neuroimage.2015.11.055

Honey, C., Kötter, R., Breakspear, M., & Sporns, O. (2007). Network structure of cerebral cortex shapes functional connectivity on multiple time scales. *Proceedings of the National Academy of Sciences of the United States of America*, *104*(24), 10240–5. https://doi.org/10.1073/pnas.0701519104

Honey, C., Sporns, O., Cammoun, L., Gigandet, X., Thiran, J., Meuli, R., & Hagmann, P. (2009). Predicting human resting-state functional connectivity from structural connectivity. *Proceedings of the National Academy of Sciences*, *106*(6), 2035–2040.

Honey, C., Thivierge, J.-P., & Sporns, O. (2010). Can structure predict function in the human brain? *NeuroImage*, *52*(3), 766–776. https://doi.org/10.1016/j.neuroimage.2010.01.071

Huang, H., & Ding, M. (2016). Linking functional connectivity and structural connectivity quantitatively: A comparison of methods. *Brain Connectivity*, *XX*(Xx), 1–10. https://doi.org/10.1089/brain.2015.0382

Huettel, S. A. (2004). *Functional magnetic resonance imaging*. (A. W. Song & G. McCarthy, Eds.). Sunderland, Mass. : Sinauer Associates, Publishers.

Hutchison, R. M., Womelsdorf, T., Allen, E. A., Bandettini, P. A., Calhoun, V. D., Corbetta, M., … Chang, C. (2013). Dynamic functional connectivity: Promise, issues, and interpretations. *NeuroImage*, *80*, 360–378. https://doi.org/10.1016/j.neuroimage.2013.05.079

Hutchison, R. M., Womelsdorf, T., Gati, J. S., Everling, S., & Menon, R. S. (2013). Resting-state networks show dynamic functional connectivity in awake humans and anesthetized macaques. *Human Brain Mapping*, *34*(9), 2154–2177. https://doi.org/10.1002/hbm.22058

Khalsa, S., Mayhew, S. D., Chechlacz, M., Bagary, M., & Bagshaw, A. P. (2014). The structural and functional connectivity of the posterior cingulate cortex: Comparison between deterministic and probabilistic tractography for the investigation of structure–function relationships. *NeuroImage*, *102*, 118–127. https://doi.org/10.1016/j.neuroimage.2013.12.022

Kjaer, T. W., Nowak, M., & Lou, H. C. (2002). Reflective self-awareness and conscious states: PET evidence for a common midline parietofrontal core. *NeuroImage*, *17*(2), 1080–1086. https://doi.org/10.1016/S1053-8119(02)91230-9

Knierim, J. J. (2015). The hippocampus. *Current Biology*, *25*(23), R1116–R1121. https://doi.org/10.1016/j.cub.2015.10.049

Koch, M. A., Norris, D. G., & Hund-Georgiadis, M. (2002). An Investigation of Functional and Anatomical Connectivity Using Magnetic Resonance Imaging. *NeuroImage*, *16*(1), 241–250. https://doi.org/10.1006/nimg.2001.1052

Kwaasteniet, B. De, Ruhe, E., Caan, M., Rive, M., Olabarriaga, S., Groefsema, M., … Denys, D. (2012). Relation Between Structural and Functional Connectivity in Major Depressive Disorder. *Biological Psychiatry*, *74*(1), 40–47.

https://doi.org/10.1016/j.biopsych.2012.12.024

Lavin, C., Melis, C., Mikulan, E., Gelormini, C., Huepe, D., & Ibañez, A. (2013). The anterior cingulate cortex: an integrative hub for human socially-driven interactions. *Frontiers in Neuroscience*, *7*(May), 64. https://doi.org/10.3389/fnins.2013.00064

Liao, X.-H., Xia, M.-R., Xu, T., Dai, Z.-J., Cao, X.-Y., Niu, H.-J., … He, Y. (2013). Functional brain hubs and their test–retest reliability: A multiband resting-state functional MRI study. *NeuroImage*, *83*, 969–982. https://doi.org/10.1016/j.neuroimage.2013.07.058

MacKay, A. L., & Laule, C. (2016). Magnetic Resonance of Myelin Water: An in vivo Marker for Myelin. *Brain Plasticity*, *2*(1), 71–91. https://doi.org/10.3233/BPL-160033

Mai, L. L., M. Young Owl, &, & M. P. Kersting. (2005). Bivariate analysis. In *Cambridge dictionary of human biology and evolution*. Cambridge, UK: Cambridge University Press.

Mazziotta, J. C., Toga, A. W., Evans, A., Fox, P., & Lancaster, J. (1995). A Probabilistic Atlas of the Human Brain: Theory and Rationale for Its Development: The International Consortium for Brain Mapping (ICBM). *NeuroImage*, *2*(2), 89–101. https://doi.org/10.1006/nimg.1995.1012

Meier, J., Tewarie, P., Hillebrand, A., Douw, L., van Dijk, B. W., Stufflebeam, S. M., & Van Mieghem, P. (2016). A Mapping Between Structural and Functional Brain Networks. *Brain Connectivity*, *31*(0), brain.2015.0408. https://doi.org/10.1089/brain.2015.0408

Michaelides, M., Anderson, S. A. R., Ananth, M., Smirnov, D., Thanos, P. K., Neumaier, J. F., … Hurd, Y. L. (2013). Whole-brain circuit dissection in free-moving animals reveals cell-specific mesocorticolimbic networks. *Journal of Clinical Investigation*, *123*(12), 5342–5350. https://doi.org/10.1172/JCI72117

Mišić, B., Betzel, R. F., de Reus, M. A., van den Heuvel, M. P., Berman, M. G., McIntosh, A. R., & Sporns, O. (2016). Network-Level Structure-Function Relationships in Human Neocortex. *Cerebral Cortex*, (April), bhw089. https://doi.org/10.1093/cercor/bhw089

Mori, S., & Van Zijl, P. C. M. (2002). Fiber tracking: Principles and strategies - A technical review. *NMR in Biomedicine*, *15*(7–8), 468–480. https://doi.org/10.1002/nbm.781

Nieuwenhuys, R. (2012). *The insular cortex. A review. Progress in Brain Research* (1st ed., Vol. 195). Elsevier B.V. https://doi.org/10.1016/B978-0-444-53860-4.00007-6

Ogawa, S., Lee, T. M., Kay, A. R., & Tank, D. W. (1990). Brain magnetic resonance imaging with contrast dependent on blood oxygenation. *Proceedings of the National Academy of Sciences of the United States of America*, *87*(24), 9868–72. https://doi.org/10.1073/pnas.87.24.9868

Park, H.-J., & Friston, K. (2013). Structural and Functional Brain Networks: From Connections to Cognition. *Science*, *342*(6158), 1238411–1238411. https://doi.org/10.1126/science.1238411

Pfefferbauma, A., Adalsteinssonc, E., Rohlfinga, T., & Sullivan, E. (2012). Diffusion tensor imaging of deep gray matter brain structures: Effects of age and iron concentration. *Neurobiol Aging*, *31*(3), 1–19. https://doi.org/10.1038/cdd.2010.172.MicroRNAs

Prasloski, T., Rauscher, A., MacKay, A. L., Hodgson, M., Vavasour, I. M., Laule, C., & Mädler, B. (2012). Rapid whole cerebrum myelin water imaging using a 3D GRASE sequence.

NeuroImage, *63*(1), 533–539. https://doi.org/10.1016/j.neuroimage.2012.06.064

Rocca, M. A., Valsasina, P., Absinta, M., Riccitelli, G., Rodegher, M. E., Misci, P., … Filippi, M. (2010). Default-mode network dysfunction and cognitive impairment in progressive MS. *Neurology*, *74*(16), 1252–1259. https://doi.org/10.1212/WNL.0b013e3181d9ed91

Roland, P. E., Geyer, S., Amunts, K., Schormann, T., Schleicher, A., Malikovic, A., & Zilles, K. (1997). Cytoarchitectural maps of the human brain in standard anatomical space. *Human Brain Mapping*, *5*(4), 222–227. https://doi.org/10.1002/(SICI)1097-0193(1997)5:4<222::AID-HBM3>3.0.CO;2-5

Rubinov, M., & Sporns, O. (2010). Complex network measures of brain connectivity: Uses and interpretations. *NeuroImage*, *52*(3), 1059–1069. https://doi.org/10.1016/j.neuroimage.2009.10.003

Seeley, W. W., Menon, V., Schatzberg, A. F., Keller, J., Glover, G. H., Kenna, H., … Greicius, M. D. (2007). Dissociable intrinsic connectivity networks for salience processing and executive control. *J Neurosci*, *27*(9), 2349–2356. https://doi.org/10.1523/JNEUROSCI.5587-06.2007

Senden, M., Deco, G., de Reus, M. A., Goebel, R., & van den Heuvel, M. P. (2014). Rich club organization supports a diverse set of functional network configurations. *NeuroImage*, *96*, 174–182. https://doi.org/10.1016/j.neuroimage.2014.03.066

Shallice, T., Fletcher, P., Frith, C. D., Grasby, P., Frackowiak, R. S. J., & Dolan, R. J. (1994). Brain regions associated with acquisition and retrieval of verbal episodic memory. *Nature*, *368*(6472), 633–635.

Shirer, W. R., Ryali, S., Rykhlevskaia, E., Menon, V., & Greicius, M. D. (2012). Decoding subject-driven cognitive states with whole-brain connectivity patterns. *Cerebral Cortex (New York, N.Y. : 1991)*, *3211*(January).

Skudlarski, P., Jagannathan, K., Calhoun, V. D., Hampson, M., Skudlarska, B. A., & Pearlson, G. (2008). Measuring brain connectivity: Diffusion tensor imaging validates resting state temporal correlations. *NeuroImage*, *43*(3), 554–561. https://doi.org/10.1016/j.neuroimage.2008.07.063

Smith, S. M., Vidaurre, D., Beckmann, C. F., Glasser, M. F., Jenkinson, M., Miller, K. L., … Van Essen, D. C. (2013). Functional connectomics from resting-state fMRI. *Trends in Cognitive Sciences*, *17*(12), 666–682. https://doi.org/10.1016/j.tics.2013.09.016

Sotiropoulos, S. N., & Zalesky, A. (2017). Building connectomes using diffusion MRI: why, how and but. *NMR in Biomedicine*, e3752. https://doi.org/10.1002/nbm.3752

Sporns, O., Honey, C., Ko, R., Sciences, B., & Neurophysiology, S. (2007). Identification and Classification of Hubs in Brain Networks, (10). https://doi.org/10.1371/Citation

Sporns, O., Tononi, G., & Kötter, R. (2005). The human connectome: A structural description of the human brain. *PLoS Computational Biology*, *1*(4), 0245–0251. https://doi.org/10.1371/journal.pcbi.0010042

Stam, C. J., & van Straaten, E. C. W. (2012). The organization of physiological brain networks. *Clinical Neurophysiology*, *123*(6), 1067–1087. https://doi.org/10.1016/j.clinph.2012.01.011

Stam, C. J., van Straaten, E. C. W., Van Dellen, E., Tewarie, P., Gong, G., Hillebrand, A., …

Van Mieghem, P. (2016). The relation between structural and functional connectivity patterns in complex brain networks. *International Journal of Psychophysiology*, *103*, 149–160. https://doi.org/10.1016/j.ijpsycho.2015.02.011

Stevens, F. L., Hurley, R. A., & Taber, K. H. (2011). Anterior Cingulate Cortex: Unique Role in Cognition and Emotion. *The Journal of Neuropsychiatry and Clinical Neurosciences*, *23*(2), 121–125. https://doi.org/10.1176/jnp.23.2.jnp121

Sun, Y., Yin, Q., Fang, R., Yan, X., Wang, Y., & Bezerianos, A. (2014). Disrupted Functional Brain Connectivity and Its Association to Structural Connectivity in Amnestic Mild Cognitive Impairment and Alzheimer ' s Disease, *9*(5). https://doi.org/10.1371/journal.pone.0096505

Suzuki, K., Yamadori, a, Hayakawa, Y., & Fujii, T. (1998). Pure topographical disorientation related to dysfunction of the viewpoint dependent visual system. *Cortex; a Journal Devoted to the Study of the Nervous System and Behavior*, *34*(4), 589–599. https://doi.org/10.1016/S0010-9452(08)70516-1

Tamminga, C. (2004). Frontal cortex function. *Am J Psychiatry*, *161*(12), 1. https://doi.org/10.1176/appi.ajp.2009.09020150

Tewarie, P., Hillebrand, A., van Dellen, E., Schoonheim, M. M., Barkhof, F., Polman, C. H., … Stam, C. J. (2014). Structural degree predicts functional network connectivity: A multimodal resting-state fMRI and MEG study. *NeuroImage*, *97*, 296–307. https://doi.org/10.1016/j.neuroimage.2014.04.038

Thomsen, C., Henriksen, O., & Ring, P. (1987). In vivo measurement of water self diffusion in the human brain by magnetic resonance imaging. *Acta Radiologica (Stockholm, Sweden : 1987)*, *28*(3), 353.

Toosy, A. T., Ciccarelli, O., Parker, G. J. M., Wheeler-Kingshott, C. A. M., Miller, D. H., & Thompson, A. J. (2004). Characterizing function-structure relationships in the human visual system with functional MRI and diffusion tensor imaging. *NeuroImage*, *21*(4), 1452–1463. https://doi.org/10.1016/j.neuroimage.2003.11.022

van den Heuvel, M. P., Kahn, R. S., Goni, J., & Sporns, O. (2012). High-cost, high-capacity backbone for global brain communication. *Proceedings of the National Academy of Sciences*, *109*(28), 11372–11377. https://doi.org/10.1073/pnas.1203593109

van den Heuvel, M. P., Mandl, C. W., Stam, C. J., Kahn, S., & Pol, H. E. H. (2010). Aberrant Frontal and Temporal Complex Network Structure in Schizophrenia : A Graph Theoretical Analysis, *30*(47), 15915–15926. https://doi.org/10.1523/JNEUROSCI.2874-10.2010

van den Heuvel, M. P., Mandl, R. C. W., Kahn, R. S., & Hulshoff Pol, H. E. (2009). Functionally linked resting-state networks reflect the underlying structural connectivity architecture of the human brain. *Human Brain Mapping*, *30*(10), 3127–3141. https://doi.org/10.1002/hbm.20737

van den Heuvel, M. P., Mandl, R., Luigjes, J., & Hulshoff Pol, H. (2008). Microstructural Organization of the Cingulum Tract and the Level of Default Mode Functional Connectivity. *Journal of Neuroscience*, *28*(43), 10844–10851. https://doi.org/10.1523/JNEUROSCI.2964-08.2008

van den Heuvel, M. P., Scholtens, L. H., Feldman Barrett, L., Hilgetag, C. C., & de Reus, M. A.

(2015). Bridging Cytoarchitectonics and Connectomics in Human Cerebral Cortex. *Journal of Neuroscience*, *35*(41), 13943–13948. https://doi.org/10.1523/JNEUROSCI.2630-15.2015

van den Heuvel, M. P., & Sporns, O. (2011). Rich-Club Organization of the Human Connectome. *Journal of Neuroscience*, *31*(44), 15775–15786. https://doi.org/10.1523/JNEUROSCI.3539-11.2011

van den Heuvel, M. P., & Sporns, O. (2013a). An Anatomical Substrate for Integration among Functional Networks in Human Cortex. *Journal of Neuroscience*, *33*(36), 14489–14500. https://doi.org/10.1523/JNEUROSCI.2128-13.2013

van den Heuvel, M. P., & Sporns, O. (2013b). Network hubs in the human brain. *Trends in Cognitive Sciences*, *17*(12), 683–96. https://doi.org/10.1016/j.tics.2013.09.012

Von Economo, C., & Koskinas, G. (1925). *Die Cytoarchitektonik der Hirnrinde des erwachsenen Menschen*. Berlin: Springer.

Walsh, M., Montojo, C. A., Sheu, Y.-S., Marchette, S. A., Harrison, D. M., Newsome, S. D., … Courtney, S. M. (2011). Object Working Memory Performance Depends on Microstructure of the Frontal-Occipital Fasciculus. *Brain Connectivity*, *1*(4), 317–329. https://doi.org/10.1089/brain.2011.0037

Whittall, K. P., Mackay, A. L., Graeb, D. A., Nugent, R. A., Li, D. K. B., & Paty, D. W. (1997). In vivo measurement ofT2 distributions and water contents in normal human brain. *Magnetic Resonance in Medicine*, *37*(1), 34–43. https://doi.org/10.1002/mrm.1910370107

Yeatman, J. D., Dougherty, R. F., Myall, N. J., Wandell, B. A., Feldman, H. M., Basser, P., … Holmes, A. (2012). Tract Profiles of White Matter Properties: Automating Fiber-Tract Quantification. *PLoS ONE*, *7*(11), e49790. https://doi.org/10.1371/journal.pone.0049790

Yuste, R. (2011). Dendritic spines and distributed circuits. *Neuron*, *71*(5), 772–781. https://doi.org/10.1016/j.neuron.2011.07.024

Zhou, F., Zhuang, Y., Gong, H., Wang, B., Wang, X., Chen, Q., … Wan, H. (2014). Altered Inter-Subregion Connectivity of the Default Mode Network in Relapsing Remitting Multiple Sclerosis : A Functional and Structural Connectivity Study, *9*(7). https://doi.org/10.1371/journal.pone.0101198

Zilles, K., Palomero-Gallagher, N., & Amunts, K. (2015). Myeloarchitecture and Maps of the Cerebral Cortex.